CONDUCTION EFFECTS IN THIN SEMICONDUCTING FILMS

by

MICHAEL ROY STINSON

B.Sc., (Honors), Simon Fraser University, 1971

A THESIS SUBMITTED IN PARTIAL FULFILLMENT OF
THE REQUIREMENTS FOR THE DEGREE OF
MASTER OF SCIENCE
in the Department
of
Physics

APPROVAL

Name: Michael R. Stinson

Degree: Master of Science

Title of Thesis: Conduction Effects
in Thin Semiconducting Films

Examining Committee:

Chairman: J. C. Irwin

R. R. Haering
Senior Supervisor

A. E. Curzon

R. F. Frindt

J. F. Cochran

Date Approved: August 3, 1973

PARTIAL COPYRIGHT LICENSE

I hereby grant to Simon Fraser University the right to lend my thesis or dissertation (the title of which is shown below) to users of the Simon Fraser University Library, and to make partial or single copies only for such users or in response to a request from the library of any other university, or other educational institution, on its own behalf or for one of its users. I further agree that permission for multiple copying of this thesis for scholarly purposes may be granted by me or the Dean of Graduate Studies. It is understood that copying or publication of this thesis for financial gain shall not be allowed without my written permission.

Title of Thesis/Dissertation:

Conduction Effects in Thin Semiconducting Films

Author:

(signature)

Michael R. STINSON

(name)

August 27, 1973

(date)

Abstract

Electron energy states, localized within a few atomic layers of a semiconductor surface, may exist within the forbidden gap; the energy band structure, over the resultant space-charge region, will be displaced relative to the Fermi level. When the thickness of such a thin film compares in magnitude to the extent of this space-charge region, marked variations in the expected conductivity will be observed. Relations are derived, expressing the conductance of thin film semiconducting slabs as a function of film thickness; a method of interpretation of experimental data in terms of the theory is discussed.

A technique is presented whereby the surface potential--the amount by which the band structure is displaced between the surface and the bulk material--can be determined. Basic to this technique is the simultaneous evaporation of several thin film slabs, of varying thickness, on the same substrate.

The theory was found capable of explaining dark conductivity measurements on thin CdS films, ranging from 800 Å to 8000 Å in thickness, at temperatures between -20°C and 60°C.

ACKNOWLEDGMENTS

I would like to thank my supervisor, Dr. R. R. Haering, for suggesting and guiding this topic to completion, and for his continuous encouragement. Drs. A. E. Curzon, R. F. Frindt and J. F. Cochran are also to be thanked for their critical reading of the manuscript.

I am grateful to Dr. R. K. Lomnes for his work in designing and building much of the apparatus, and to Mr. J. Mercier for his invaluable technical assistance.

I appreciate very much the help of Margaret Linquist, Georgina Carlson and Jenny Clemente for the typing of the thesis.

Finally, I would like to acknowledge the financial support of the National Research Council.

TABLE OF CONTENTS

LIST OF TABLES

LIST OF ILLUSTRATIONS

1. Introduction

In a large semiconductor sample of uniform composition the conductivity (or, the conductivity tensor) may be considered independent of position; any effects ascribed to the surface will be negligible. However, when any sample dimension becomes very small--as is the case of thin films--surface effects will become more important. First, surface scattering may give rise to a reduced mobility near the surface; second, and more important to this study, there may be localized energy levels in the surface region--these, as will be seen, will cause local variations in the conductivity.

This study, then, is concerned with the theoretical and experimental effects of surface states on the conduction current in thin semiconducting films.

1.1 Origin of the Space-Charge Region

The sample geometry utilized throughout most of this thesis is depicted in Fig. 1-1, wherein the resistance across the length ℓ of the sample is being measured; the thickness t, is much less than either the length ℓ or the width ω.

A possible energy structure for such an n-type semiconducting film is shown in Fig. 1-2a, for the case of the surface having no effect on the band structure. This is not realistic; the surface atoms are in an obviously different

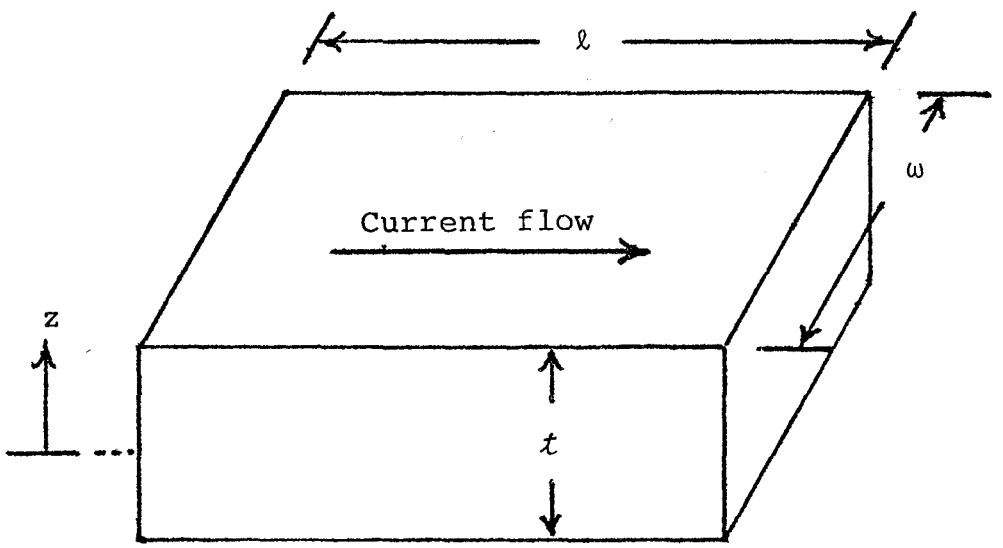

Figure 1-1. Sample geometry

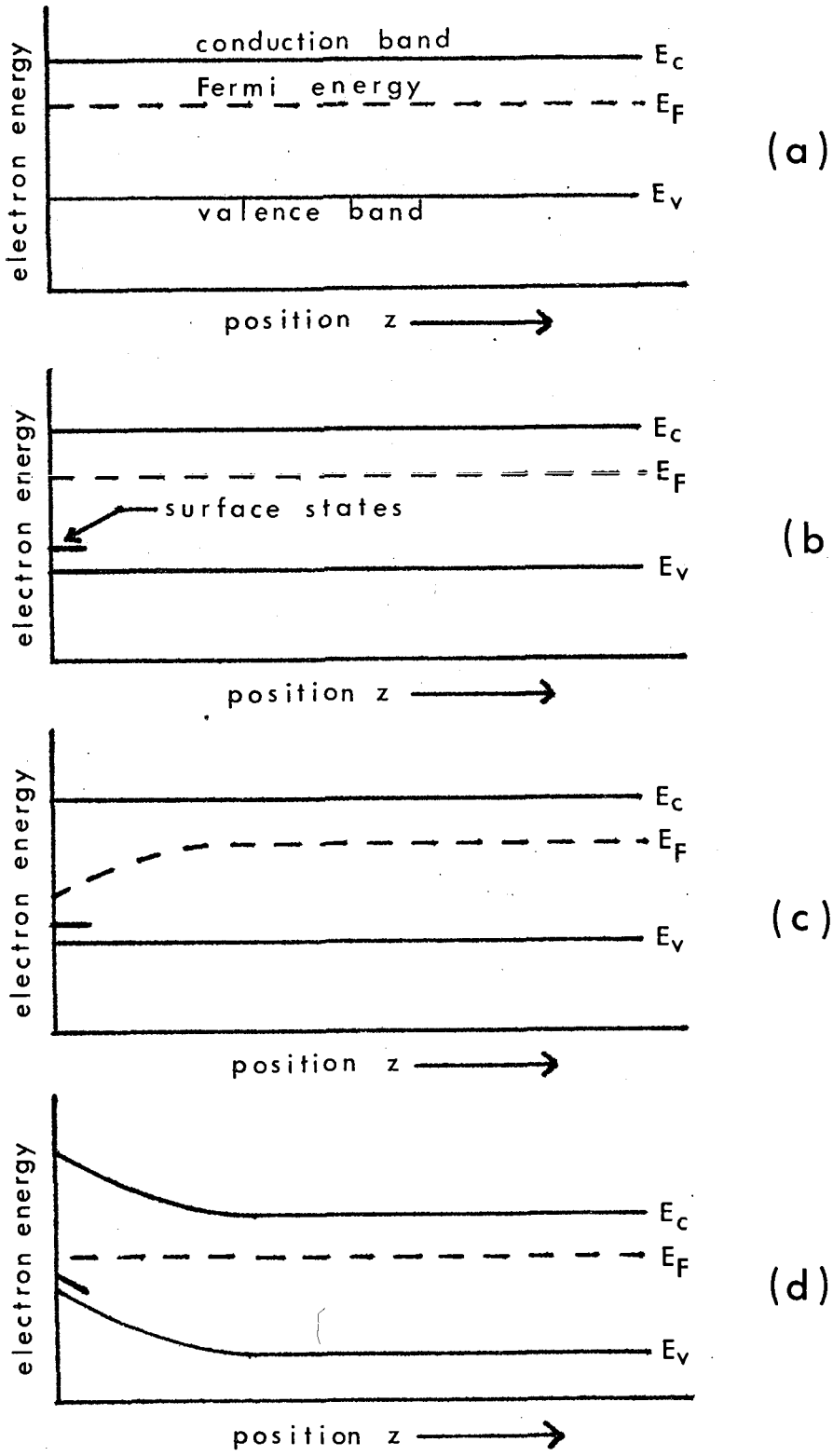

Figure 1-2. The origin, shown schematically, of the space-charge region.

environment than the bulk atoms. There could be different chemical species adhered to the surface, or even if the surface is clean and exposed to a vacuum the sudden termination of the lattice will cause a local variation in the wave function $\psi(\vec{r})$.

Suppose the effect of the surface (or interface between the semiconductor and surrounding species) is to introduce localized acceptor-like energy levels within several atomic layers of the surface--this is depicted in Fig. 1-2b. Since electrons will tend to drop down from the conduction band and populate these levels, the Fermi level must shift so that it is nearer to these states, as in Fig. 1-2c. To end this progression, it is considered that the Fermi level must be constant throughout the sample in thermal equilibrium; the resultant energy structure is pictured in Fig. 1-2d, all bands bending to preserve both the constancy of the Fermi level, and the necessary variation at the surface of the relative position of the Fermi level. The region of the localized acceptor levels is the surface region; the region in which the energy bands bend is the space-charge region.

Similar arguments will apply to p-type semiconductors, where holes are the majority carriers.

A space-charge region like that in Fig. 1-2d, where there will be a shortage of majority-carriers, is termed a depletion region. Similarly, if the effect of surface states is to bend the bands in the opposite direction (that is, donor-like surface

states), an accumulation region arises, where the number of majority carriers is increased.

1.2 Historical Outline

It is commonly accepted now that surface states give rise to a potential at the surface of semiconductors. This idea was first proposed by Bardeen[1] in 1947, to explain certain data on the rectification characteristics of metal-semiconductor and semiconductor-semiconductor junctions. This superceded the previous explanation of potential barriers being due to the difference in contact potential of the two materials. Theoretical models of surface states had been proposed earlier by Tamm[2] and Schockley[3]. More recent and detailed theoretical studies of these localized energy states include such work as that by Heine[4], describing the derivation of the appropriate wave-functions.

Among the earliest works confirming the existence of, and describing, the space-charge region are papers by Bardeen and Morrison[5] in 1954, and Statz and DeMars[6] in 1958. In particular, Bardeen and Morrison were able to control the surface potential reproducibly by varying the gaseous ambient surrounding a semiconductor; the magnitudes of the surface potentials were determined by observing surface conductances, with an electric field applied normal to the surface. Further

experimental techniques are described in the book by Many, Goldstein and Grover[7], and in the article by Mark[8].

Theoretical treatment of the space-charge region has kept pace with experimental work; the basic concern is the shape of the potential within the sample. Among the first papers published were those by Kingston and Neustadter[9] in 1955, and by Seiwatz and Green[10] in 1958--the latter discuss the problem quite generally, allowing for partially ionized donor and acceptor levels, and degeneracy in the conduction and valence bands. Later papers discuss various approximations, applicable in special circumstances, and the relationship between the surface potential and the localized surface states.

There has been similar work, both theoretical and experimental, on the mobility near the surface of semiconductors. As well as the contribution of surface scattering, the mobility will be influenced by the form of the surface potential. Schrieffer[11] in 1955 began the theoretical work on mobility in surface-space charge layers.

Research at present is continuing along the same lines, desiring an accurate picture of how surface states modify the bulk properties of semiconductors.

1.3 Origin of Surface States

In this thesis the explicit nature and origin of surface

states is not considered in any detail--rather, it is the resultant space-charge region and its effect on conduction that is dealt with. Such references as Many, Goldstein and Grover[7] and Davison and Levine[12] describe the development of the theory of surface states quite well; some of the basic ideas are presented in the next paragraphs.

The band structure of a semiconductor is obtained from a solution of Schrödinger's wave equation, as applied to an infinite lattice[13]; this will describe the interior of a relatively large sample. However, the atoms near the surface are obviously in an altered environment--new boundary conditions apply to the wave equation. As a result of the termination of the lattice, the surface atoms will also be displaced from their expected lattice sites.

In an infinite lattice, the values of the wavevector $\vec{k}$ are by necessity real; when the lattice is terminated, however, complex values of $\vec{k}$ are allowable, such that the corresponding wave functions are damped outside the surface region. From theoretical work, such as the original proposals by Tamm[2], it is known that quantum states, localized near the surface, can arise, their energies falling within the forbidden gap of the semiconductor considered.

These "Tamm states" may exist even on a perfect crystal. In addition, the surface will have layers of other adsorbed species; this will further complicate the issue. Additional

interface states due to the interaction of semiconductor surface and adsorbed layers may arise.

Allowing surface states (of electrons) localized in the first few atomic layers, the curved band structures described in section 1.1 are possible.

1.4 Objectives of this Study

In a semiconducting film whose thickness is of the same order as the extent of the space-charge region, the effective measured conductivity will differ from the bulk value. In a depletion-type space-charge region, the semiconductor can be assumed depleted of carriers within a distance d_o of the surface; as used by Haering and O'Hanlon[14] the conductance will have the form

$$G = \frac{\omega\sigma_b}{\ell} (t-2d_o) \ , \qquad (1\text{-}1)$$

where σ_b is the bulk conductivity. This equation is also applicable to accumulation layers, d_o being negative. Whatever the nature of the space-charge region, though, equation (1-1) is an approximation. In the following study the exact form of conductance dependence on sample thickness is determined. The effect of the surface states is characterized by a surface potential V_s, the amount by which the energy bends are shifted

in the space-charge region.

Some experimental results obtained were analyzed in terms of the theory developed. This was done, not so much to study surface states or a particular semiconductor, but as a check on the theory of the space-charge region. These results are described in Chapter 4.

In Chapter 5 the capability of the theory to describe experimental results is discussed, and other conclusions presented.

2. Theory of Conduction in Thin Semiconducting Films

2.1 Introduction

In the previous chapter a potential at the surface of a semiconductor was seen to arise with the introduction of surface/interface states. This chapter will assume the surface potential is known and deduce, from this, the effects on conduction measurements in thin films. The form of the potential is determined, from which can be obtained the dependence of conductance (parallel to the plane of the film) on the film thickness. A method of analysis of such experimental results is introduced to allow the determination of various surface and bulk properties. In particular, a method, unmentioned in the literature, is described which allows the surface potential V_s to be measured.

The geometry of Fig. 1-1 again applies, current flow being in the x-y plane. The details of the energy structure are shown in Fig. 2-1. E_c and E_v are the energies corresponding to the conduction and valence band edges, respectively; E_F is the Fermi energy of the system, with E_i being the corresponding intrinsic Fermi energy. The energies $E_{D\ell}$ and E_{Aj} refer, respectively, to the ℓ^{th} donor level and the j^{th} acceptor level.

The potential qV is introduced as a measure of the bending of the energy bands, with q being the magnitude of the electron charge; V may then be defined through

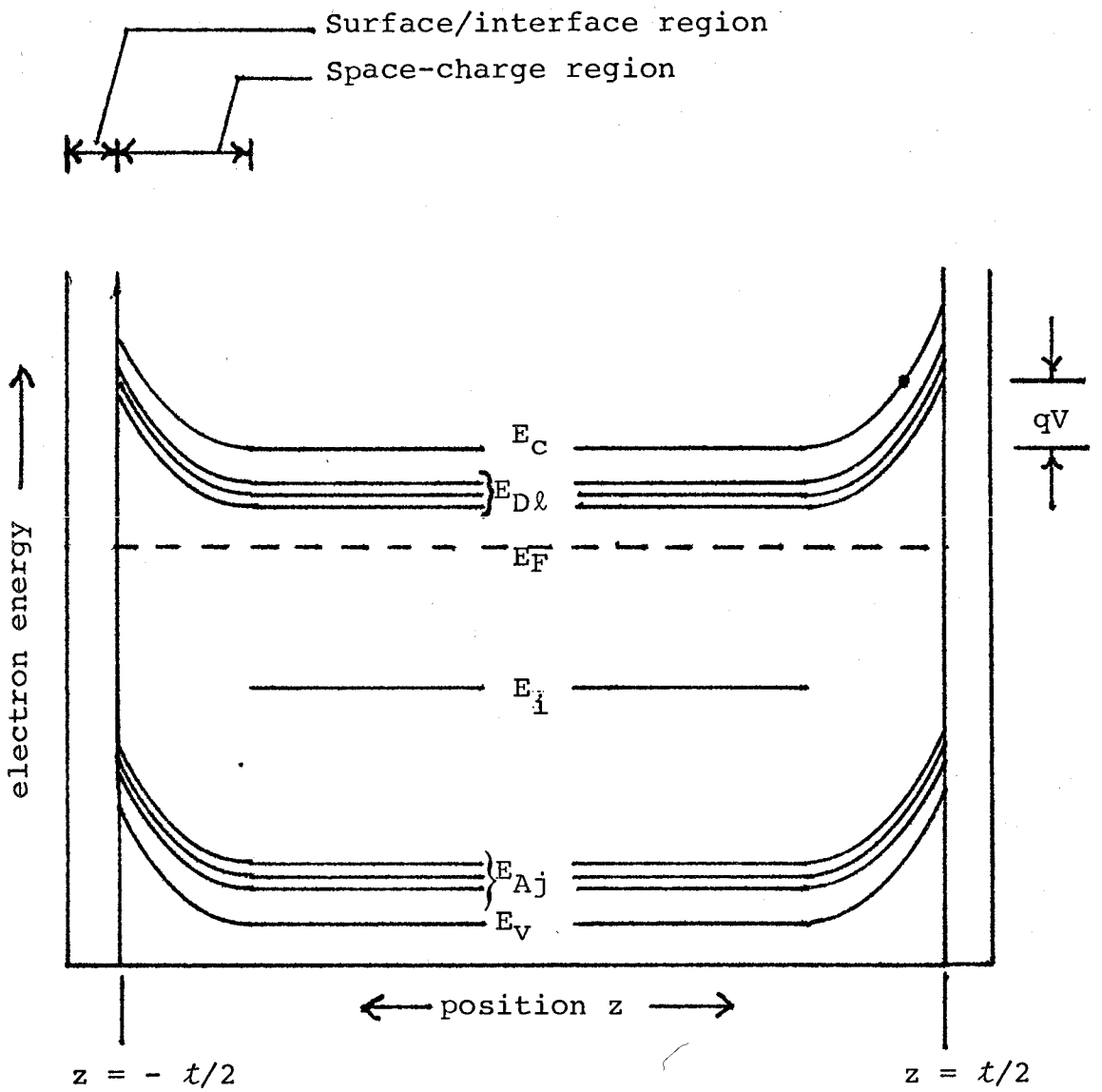

Figure 2-1. Energy structure of the thin film semiconductor

$$qV = (E_c)_b - E_c. \qquad (2\text{-}1)$$

Here, as in the remainder of this study, the subscript b refers to the value of the parameter being discussed in the bulk material. Note that qV is negative when the energy bands bend in the direction of positive electron energy.

It is convenient to work with dimensionless variables; hence, a reduced potential v is introduced:

$$v = \frac{qV}{kT}, \qquad (2\text{-}2)$$

with T being the absolute temperature of the sample, k being Boltzmann's constant.

This study will be concerned with n-type semiconducting thin films; the extension to p-type material does not involve any new principles and is not included. The temperatures being considered range between -20°C and 60°C.

2.2. Application of Poisson's Equation to Semiconductor Statistics

The shape of the electric potential throughout the sample is obtained from a solution of Poisson's equation. For the geometry shown in Fig. 1-1, and assuming the sample has a uniform chemical composition, Poisson's equation takes the

form

$$\frac{d^2V(z)}{dz^2} = -\frac{\rho(z)}{\kappa\varepsilon_o} , \qquad (2-3)$$

where κ is the dielectric constant and ε_o is the permittivity of free space; $\rho(z)$ is the free charge density, which will include both free carriers and ionized donor and acceptor atoms.

In this section of theory $\rho(z)$ will be expressed in terms of the potential $V(z)$ and several bulk parameters, thus allowing equation (2-3) to be integrated. This calculation has been done (see, for example, Kingston and Neustadter[9] or Seiwatz and Green[10]) previously in the literature under varying boundary conditions, and varying degrees of donor level ionization. Since the combination of incomplete donor level ionization and thin (in the z-direction) semiconducting films is not dealt with in the literature, a complete presentation will be given here.

If n and p represent the densities, respectively, of electrons in the conduction band and holes in the valence band, and if $N_{D\ell}^{+}$ and N_{Aj}^{-} represent the densities, respectively, of ionized donor sites with energy $E_{D\ell}$ and ionized acceptor sites with energy E_{Aj}, then $\rho(z)$ may be expressed as

$$\rho = q[-n + p + \sum_{\ell} N_{D\ell}^{+} - \sum_{j} N_{Aj}^{-}] . \qquad (2-4)$$

For the case of non-degenerate statistics, where both $|E_c-E_F|$ and $|E_F-E_v|$ exceed $3kT$, the free carrier densities may be represented by[15]

$$n = N_c \exp -[\frac{E_c - E_F}{kT}], \text{ and } p = N_v \exp -[\frac{E_F - E_v}{kT}], \tag{2-5}$$

where,

$$N_c = 2[\frac{2\pi m_n kT}{h^2}]^{3/2}, \; N_v = 2[\frac{2\pi m_p kT}{h^2}]^{3/2}; \tag{2-6}$$

here, h is Planck's constant, and m_n and m_p are the effective masses of electrons in the conduction band and holes in the valence band. Implicit in equations (2-5) and (2-6) is the assumption that the semiconductor has spherical or elliptical energy surfaces[10].

Similarly, the densities of ionized donors and acceptors are given by [16]

$$N_{D\ell}^{+} = N_{D\ell} - \frac{N_{D\ell}}{1 + \frac{1}{g_{D\ell}} \exp \frac{E_{D\ell} - E_F}{kT}} \tag{2-7a}$$

$$\text{and } N_{Aj}^{-} = N_{Aj} - \frac{N_{Aj}}{1 + g_{Aj} \exp \frac{E_F - E_{Aj}}{kT}}, \tag{2-7b}$$

where $N_{D\ell}$ and N_{Aj} are the densities of donor and acceptor sites, and $g_{D\ell}$ and g_{Aj} are the degeneracies of the energy levels $E_{D\ell}$ AND E_{Aj}. Combining equations (2-2) to (2-7), Poisson's equation becomes

$$\frac{d^2v}{dz^2} = \frac{q^2}{\kappa\varepsilon_o kT}\left\{N_c \exp -\left[\frac{E_c - E_F}{kT}\right] - N_v \exp -\left[\frac{E_F - E_v}{kT}\right] - \sum_{\ell} \frac{N_{D\ell}}{1 + g_{D\ell}\exp\left[\frac{E_F - E_{D\ell}}{kT}\right]} + \sum_{j} \frac{N_{Aj}}{1 + \frac{1}{g_{Aj}}\exp\left[\frac{E_{Aj} - E_F}{kT}\right]}\right\} \tag{2-8}$$

Equation (2-8), as it now stands, could be used to calculate the potential for n-type, p-type or compensated semiconducting films. This study, however, is concerned solely with n-type semiconductors; this restriction allows equation (2-8) to be simplified. For n-type material the Fermi level will be sufficiently far removed from the acceptor bands that they will be completely ionized; as well, there may be some donor levels (particularly those near the conduction band) which may also be very nearly completely ionized. In equation (2-8) allow the summation over ℓ to be separated into a summation over ℓ' for those donor levels fully ionized, and a summation over i for the levels of incomplete ionization; this gives

$$\frac{d^2v}{dz^2} = \frac{q^2}{\kappa\varepsilon_o kT}\left\{N_c \exp -\left[\frac{E_c - E_F}{kT}\right] - N_v \exp -\left[\frac{E_F - E_v}{kT}\right] - \sum_{\ell'} N_{D\ell'} + \sum_{j} N_{Aj} - \sum_{i} \frac{N_{Di}}{1 + g_{Di}\exp\left[\frac{E_F - E_{Di}}{kT}\right]}\right\}. \tag{2-9}$$

Equation (2-9) is still not in a form suitable for integration since both $(E_c - E_F)$ and $(E_F - E_v)$ are dependent on v; further manipulation of equation (2-8) follows in the next section of theory.

2.3 The Determination of the Potential

Equation (2-9) can be further simplified if written in terms of certain bulk parameters. Suppose the surface states were such that the energy bands of Fig. 2-1 extended to the surface without being bent up or down; equation (2-9) would still be applicable, with all parameters referring to the bulk material--the semiconductor would be essentially bulk material right up to the surface. Now, though, the term $\frac{d^2v}{dz^2}$ would be zero. Hence, a subsidiary equation to (2-9) is

$$0 = N_c \exp -\left[\frac{(E_c - E_F)_b}{kT}\right] - N_v \exp\left[-\frac{(E_F - E_v)_b}{kT}\right] - \sum_{\ell'} N_{D\ell'} + \sum_j N_{Aj} - \sum_i \frac{N_{Di}}{1 + g_{Di} \exp \frac{(E_F - E_{Di})_b}{kT}} , \qquad (2\text{-}10)$$

where again the subscript b refers to that parameter in the bulk. Substituting this back into equation (2-9) to remove the terms $(\sum_{\ell'} N_{D\ell'})$ and $(\sum_j N_{Aj})$, and utilizing equations (2-1) and (2-2), it is found that

$$\frac{d^2v}{dz^2} = \frac{q^2}{\kappa\varepsilon_o kT}\left[n_b e^v - n_b - p_b e^{-v} + p_b + \sum_i N_{Di}\left(\frac{1}{1+\frac{1}{g_{Di}} e^{x_i - v}} - \frac{1}{1+\frac{1}{g_{Di}} e^{x_i}}\right)\right], \qquad (2\text{-}11)$$

where x_i is defined by

$$x_i \equiv \frac{(E_{Di}-E_F)_b}{kT} \quad . \tag{2-12}$$

If no donors or acceptors were present the Fermi energy would have an intrinsic value given by[15]

$$E_i \equiv \frac{1}{2}(E_c + E_v) - \frac{1}{2} kT \ln \frac{N_c}{N_v} \; ; \tag{2-13}$$

typically, E_i is located near the middle of the band gap. It is now convenient to define a bulk potential u_b as

$$u_b \equiv \frac{(E_F-E_i)_b}{kT} \quad . \tag{2-14}$$

Equation (2-14) can be used to re-express equation (2-11) in a more convenient form. Thus,

$$\frac{d^2v}{dz^2} = \frac{1}{L^2}\left[\frac{\sinh(u_b+v)-\sinh u_b}{\cosh u_b} + \sum_i \frac{N_{Di}}{n_b+p_b}\left(\frac{1}{1+\frac{1}{g_{Di}}e^{x_i-v}} - \frac{1}{1+\frac{1}{g_{Di}}e^{x_i}}\right)\right] \tag{2-15}$$

where

$$L^2 \equiv \frac{\kappa\varepsilon_o kT}{q^2(n_b + p_b)} \tag{2-16}$$

The parameter L is the effective Debye length; it is a direct measure of the extent of the space-charge region[7]. In this study a typical value for L would be 2000 Å.

Poisson's equation has now been expressed in a form suitable for integration.

It will be assumed that the semiconducting film (Fig. 1-1) is symmetric about $z = 0$; this is not unreasonable since the physical environments of the opposite surfaces, $z = \pm t/2$, can be made quite similar. Hence at $z = 0$ it follows that $\frac{dv}{dz} = 0$; further, define v_o as the value of the potential at $z = 0$. Carrying through one integration of equation (2-15) it is obtained that

$$\frac{dv}{dz} = \pm \sqrt{2}\, \frac{F(v,v_o)}{L} \quad , \tag{2-17}$$

where the function $F(v,v_o)$ is given by

$$F^2(v,v_o) \equiv \left\{ \frac{\cosh(u_b+v)-\cosh(u_b+v_o)}{\cosh u_b} - (v-v_o) \tanh u_b \right.$$

$$\left. - \sum_i \left[\frac{N_{Di}}{n_b+p_b} \frac{(v-v_o)}{1+\frac{1}{g_{Di}} e^{x_i}} - \frac{N_{Di}}{n_b+p_b} \ln\left(\frac{e^{v}+\frac{1}{g_{Di}} e^{x_i}}{e^{v_o}+\frac{1}{g_{Di}} e^{x_i}} \right) \right] \right\} \tag{2-18}$$

In equation (2-17) the assigning of the + or - depends on the sign of z and the sign of v_o; since, in the following work, it will be obvious which sign to choose, the conditions determining the sign in equation (2-17) will not be detailed. The effective Debye length, L, which characterizes the bending of the energy bands is seen to enter equation (2-17) quite simply.

A numerical integration of equation (2-17) could be made to obtain the shape of the potential v(z). Since the actual variation of v(z) is not essential to the future sections of theory and thus, only of incidental interest, examples of such curves are not displayed. They appear, qualitatively, as depicted in Figure 2-1; actual examples may be seen in such references as Dousmanis and Duncan[17].

2.4 Theoretical Dependence of Conductance on Thickness

This study is directed toward obtaining the expected modification of sample conductance caused by changes in carrier density near the surface of the material.

Consider a sample as in Fig. 1-1, where current flows in the x-direction. For a sample with length ℓ, width ω and thickness t, with both ω and ℓ being much larger than L or t, the measured conductance, G, is

$$G = \frac{\omega}{\ell} \int_{-t/2}^{+t/2} \sigma(z)\, dz \qquad (2\text{-}19)$$

It will now be assumed that the electrons, the majority carriers, will completely dominate the holes in making up the conductance; it is then necessary to restrict the range of v since values too strongly negative will result in a greater domination by the holes (noting that $n = n_b e^{v}$, $p = p_b e^{-v}$). Also, the mobility

μ is assumed to be constant throughout the semiconductor; this is tenable when it is considered that the thermal mean free path[7] ($\lambda \approx \mu/q\ [3m_n kT]^{\frac{1}{2}}$) for CdS is less than 90 Å at room temperature--in fact, values of $\lambda < 10$ Å were found for the samples being worked with in the experimental chapter; hence, μ will be about the same to within ten Angstroms of the surface. The conductivity can then be expressed as

$$\sigma(z) = n(z)\ q\mu \quad . \tag{2-20}$$

Utilizing the fact that $n(z) = n_b\ e^{v(z)}$, and that $(n_b q\mu)$ is the bulk conductivity σ_b, then equations (2-19) and (2-20) give

$$G = 2\frac{\omega}{\ell}\int_o^{t/2} \sigma_b\ e^{v(z)}\,dz \quad , \tag{2-21}$$

where the symmetry of the sample has been incorporated. Converting equation (2-21) to an integral over v--using $dz = (\frac{dz}{dv})dv$ and the expression for $(\frac{dv}{dz})$ in equation (2-17) it is found that

$$\frac{\ell}{\omega}\frac{G}{\sigma_b L} = \pm\sqrt{2}\int_{v_o}^{v_s} \frac{e^v dv}{F(v,v_o)} \quad , \tag{2-22}$$

where the sign is chosen unambiguously to give a positive conductance.

A numerical integration of equation (2-22) results in the theoretical determination of the conductance. In such a calculation v_s, the reduced potential at the surface, would be assumed known--it can, under appropriate conditions, be determined experimentally. v_o, the potential at $z = 0$, is not arbitrary but determined by the thickness t of the sample. This is seen by a rearrangement of equation (2-17) to give

$$t/L = \pm \sqrt{2} \int_{v_o}^{v_s} \frac{dv}{F(v, v_o)} \quad , \qquad (2\text{-}23)$$

where the sign is chosen to make t positive.

An experimental approach to the measurement of surface potentials is now evident. If several samples of identical chemical composition and preparation, but with different thicknesses are prepared, a plot of $\frac{\ell}{\omega} \frac{G}{\sigma_b L}$ versus t/L can be constructed experimentally; a comparison with similar theoretical curves can then be made, and information about the surface obtained. The appropriate tools necessary to enact this comparison are developed in the following section of theory.

Concerning the above discussion it is expected that the surface potential V_s will be the same for the samples of different thicknesses. The potential will be dependent upon the density of surface states and their occupation statistics: it is the surface region which determines V_s, the rest of the sample

merely adjusting its electron distribution to satisfy Poisson's equation and semiconductor statistics.

In Fig. 2-2 are shown examples of the theoretical variation of $\frac{\ell}{\omega}\frac{G}{\sigma_b L}$ with t/L; for these it was assumed that the donor levels were completely ionized, with $u_b = 10$. Several features are evident which are shared by all such curves: the curves are approximately linear for both $t<<L$ and $t>>L$; the transition between these two occurs near $t = L$.

The space-charge region is an accumulation layer when $V_s>0$, and a depletion layer when $V_s<0$. The measured conductivities will not conform to the relation $\sigma = \frac{\ell}{\omega}\frac{G}{t}$, but will be larger (for accumulation layers) or smaller (for depletion layers).

The slope of the $\frac{\ell}{\omega}\frac{G}{\sigma_b L}$ versus t/L curve is 1 at large values of t, which is the expected bulk behaviour. A correct determination of conductivity requires knowing the rate change of conductance with thickness when $t>>L$. When the sample thickness is comparable with L it is essential to form a G versus t curve and deduce σ_b from this.

2.5 The Parameterization of Conductance-thickness Curves

Rather than attempting to match experimental and theoretical conductance-thickness curves point for point, it is by far more convenient to characterize such curves by appropriate parameters, and then to match these parameters.

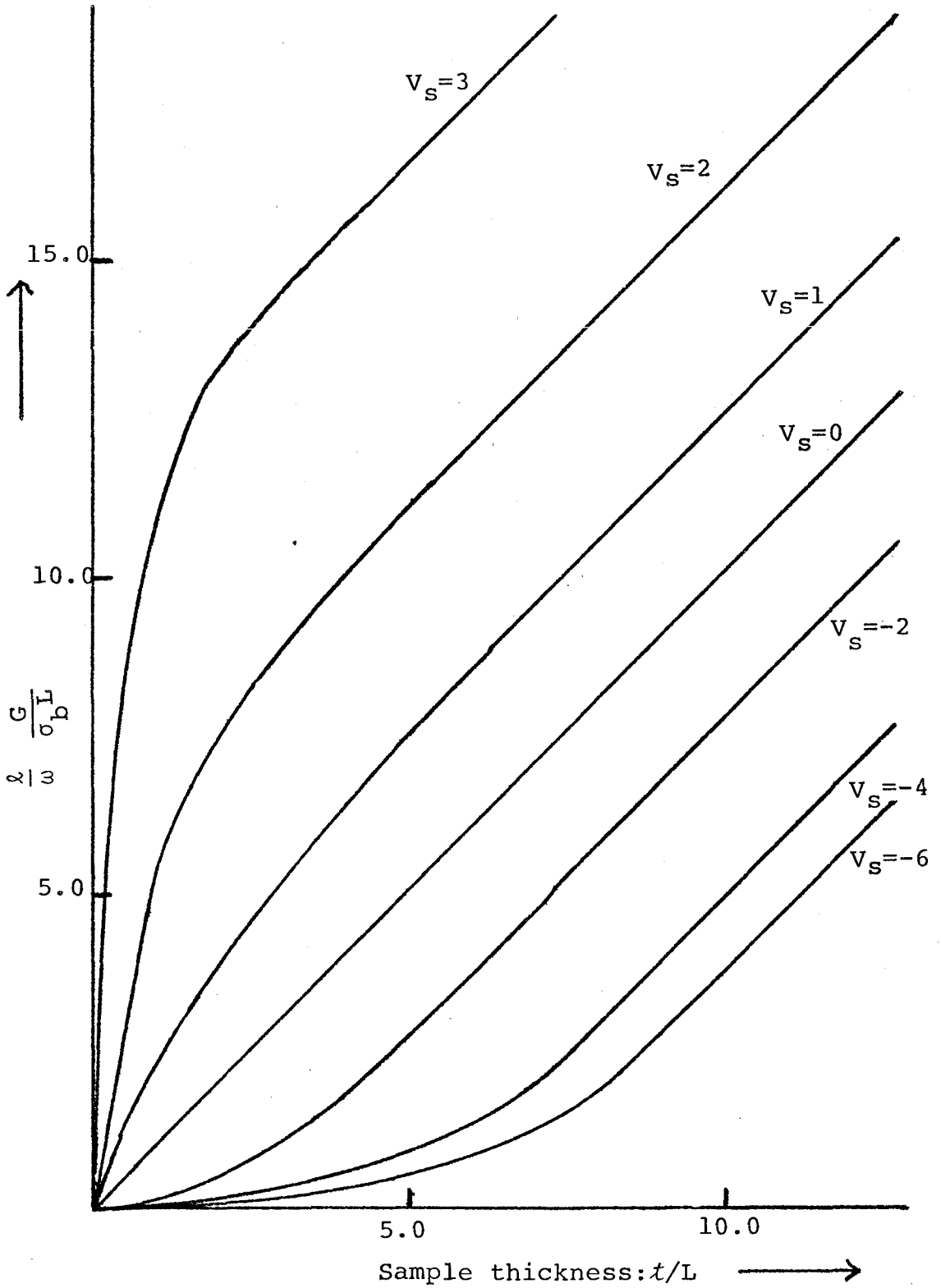

Figure 2-2. Theoretically predicted dependence of conductance on sample thickness.

Consider a plot of $\frac{\ell}{\omega} G$ against t. The first obvious parameter is σ_b, the slope of the curve at large sample thicknesses. A second parameter is the slope of the curve near $t = 0$--this, as will be seen, is most useful: consider a sample whose thickness t' is approaching zero--simultaneously, v_o will be approaching v_s, so that $\Delta v \equiv v_s - v_o$ is approaching zero. Then,

$$\frac{\ell}{\omega} \frac{dG}{dt} \Big|_{t=0} = \frac{\ell}{\omega} \lim_{t' \to 0} \left[\frac{G(t')}{t'} \right] \tag{2-24}$$

In equation (2-22) the integrand $\frac{e^v}{F(v,v_o)}$ may be expanded into powers of $(v-v_o)$--a Taylor series expansion--and for small values of $(v_s - v_o)$ an approximate solution to the integral may be found:

$$\frac{\ell}{\omega} \frac{G}{\sigma_b L} \approx \sqrt{2}\, e^{v_o}\, a_o\, (v_s - v_o)^{\frac{1}{2}} \quad , t' \to 0, \tag{2-25}$$

where a_o is a constant dependent upon v_o, $\frac{N_{Di}}{n_p + p_b}$, g_{Di}, u_b, and x_i. A similar expansion and integration can be performed using equation (2-23) to give

$$t'/L \approx \sqrt{2}\, a_o\, (v_s - v_o)^{\frac{1}{2}}, \quad t' \to 0, \tag{2-26}$$

where this a_o is identical to that in equation (2-24); hence, from equation (2-24) noting that $v_o \to v_s$ as $t' \to 0$,

$$\frac{\ell}{\omega} \frac{dG}{dt} \Big|_{t=0} = \sigma_b\, e^{v_s} \,. \tag{2-27}$$

This result might be expected intuitively: as $t' \to 0$, the electron concentration will be almost uniform, being given by (see equation 2-5) $n = N_c \exp - \left[\frac{(E_c)_b - qV_s - E_F}{kT}\right]$; equation (2-27) follows from this almost immediately.

The reduced surface potential v_s is an easily determined parameter: e^{v_s} is the ratio of the slopes (of an $\frac{\ell}{\omega} G$ versus t curve) at very small and very large sample thicknesses. Experimentally, several samples of identical chemical composition but varying thicknesses are prepared--presumably (as discussed in the previous section of theory) v_s will be the same for each. By constructing a plot of conductance versus thickness, the surface potential v_s is then easily found. Results obtained using this technique are discussed later.

Although the technique described above is very useful, it should be noted that the curves have not yet been uniquely specified. Complete specification would require quite a few more characterizing parameters, and the increased knowledge (of only bulk parameters) would not be worth the increased work. Only one more parameter will be introduced; in this study, this parameter's main use will be to develop an experimental check on the developed theory.

For large thicknesses the conductance varies linearly with sample thickness, having the form

$$\frac{\ell}{\omega} G = \sigma_b \, (t - 2d_o) \quad , \quad t >> L. \tag{2-28}$$

The asymptotic intercept, $2d_o$, is the third parameter used to characterize the conductance-thickness curves. It may be

defined as

$$2d_o = \lim_{t\to\infty}\left[t - \frac{\ell}{\omega}\frac{G(t)}{\sigma_b}\right] . \qquad (2\text{-}29)$$

Realizing that v_o tends to zero when $t\to\infty$, and using equations (2-22) and (2-23) one obtains the expression

$$d_{o/L} = \pm \frac{\sqrt{2}}{2}\int_o^{v_s}\frac{(1-e^v)dv}{F(v,0)} \qquad (2\text{-}30)$$

where the sign of d_o/L is chosen to be opposite that of v_s, and where the function $F(v,0)$ is the value of $F(v,v_o)$ evaluated at $v_o = 0$; from equation (2-18) it is seen that

$$F^2(v,0) = \left\{\frac{\cosh(u_b+v)-\cosh u_b}{\cosh u_b} - v\tanh u_b - \sum_i\left[\frac{N_{Di}}{n_b+p_b}\frac{v}{1+\frac{1}{g_{Di}}e^{x_i}} - \frac{N_{Di}}{n_b+p_b}\ln\frac{e^v+\frac{1}{g_{Di}}e^{x_i}}{1+\frac{1}{g_{Di}}e^{x_i}}\right]\right\} \qquad (2\text{-}31)$$

The three parameters, σ_b, v_s and $2d_o$, may be used to describe theoretical and observed curves of G versus t; their origins are summarized in Figure 2-3. The only information, using these techniques, about the surface states that can be obtained is the height of the surface barrier v_s; the detailed energy structure of the surface states must be deduced using other techniques[7,8,12]. The technique presented in this study, although not providing specific details about the surface, has the utility of predicting several bulk properties by an appropriate analysis of d_o and v_s. This aspect is developed in the following section.

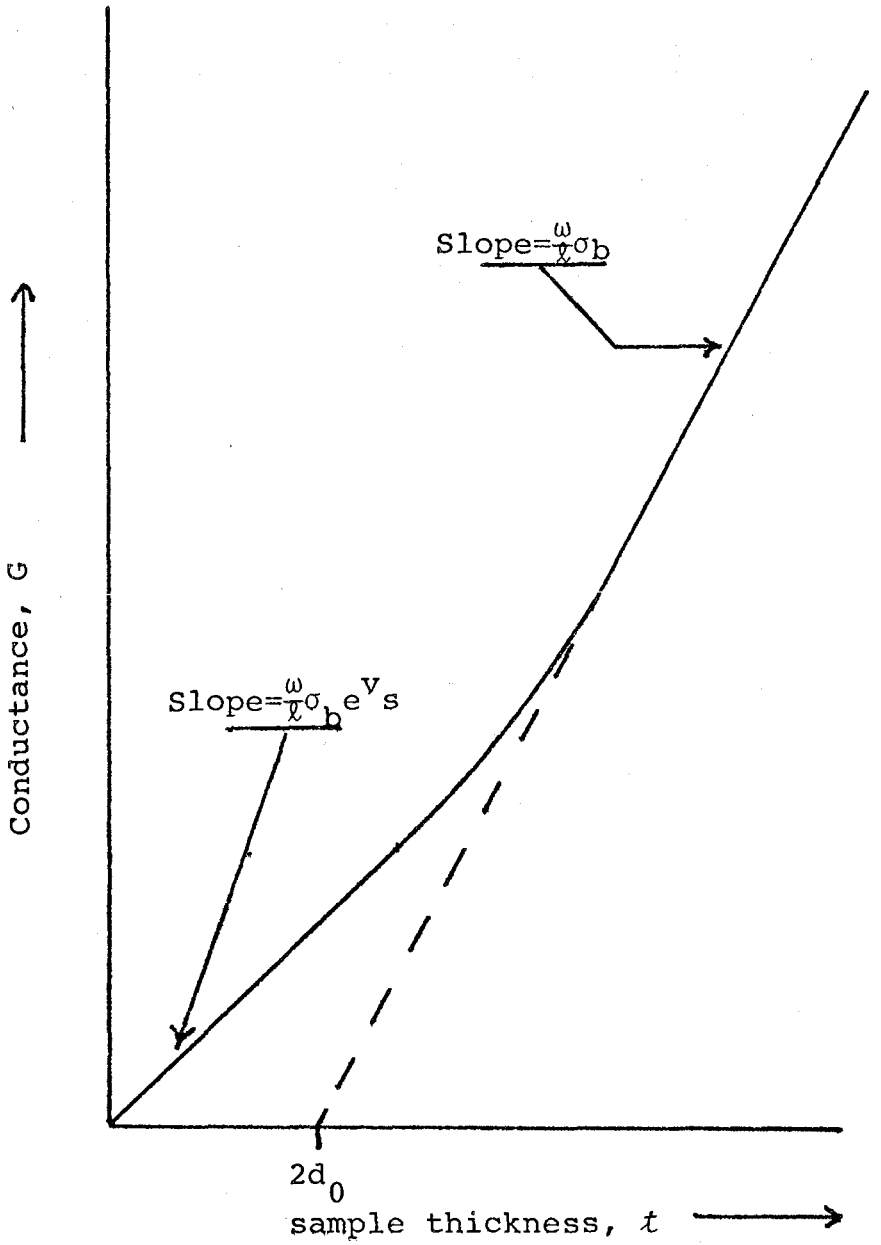

Figure 2-3. Summary showing, schematically, the origin of the parameters: σ_b, $2d_0$ and v_s.

2.6 Temperature Dependence

In a typical set of samples only one set of values--σ_b, v_s and $2d_o$--can be deduced, at a particular temperature. This, in itself, would not be sufficient to provide a comparison with the theory developed. On the other hand, if several different sets of samples were made up (that is, by separate evaporations) there would be no assurance that they had identical physical make-ups.

To properly check the theory developed it is desirable to have several values of v_s available to work with, all for the same sample. The reduced potential, v_s, can be varied (after the sample preparation) by several means: variations in the ambient atmosphere [5], or the application of an electric field normal to the surface [6]. However, in the experimental portion of this study, v_s was easily varied by changing the temperature--in equation (2-2), if the surface potential V_s is roughly constant then v_s will vary inversely with temperature. This section of theory discusses, then, the temperature dependence of the characterizing parameters.

Combining equations (2-30) and (2-16) it is found that

$$d_o^2 = \frac{1}{2}\left[\int_o^{v_s} \frac{(1 - e^{v})\,dv}{F(v,o)}\right]^2 \frac{\kappa\varepsilon_o kT}{q^2(n_b + p_b)}; \qquad (2\text{-}32)$$

Assuming $n_b >> p_b$, and substituting for n_b from equation

(2-5)

$$d_o^2 = \tfrac{1}{2}\left[\int_o^{V_s} \frac{(1 - e^V)\,dv}{F(v,o)}\right]^2 \left(\frac{\kappa\varepsilon_o}{q^2}\right)\frac{kT}{N_c}\exp\left[\frac{(E_c - E_F)}{kT}\right] . \qquad (2\text{-}33)$$

The effective density of states N_c also has some temperature dependence, as seen in equation (2-6); it is convenient to define a temperature independent parameter, N_c', by

$$N_c' = 2\left[\frac{2\pi m_n}{h^2}\right]^{3/2}; \quad N_c = N_c'(kT)^{3/2} \qquad (2\text{-}34)$$

For CdS, with $m_n = 0.165\ m_e$, $N_c' = 4.05 \times 10^{20}\ (ev)^{-3/2}\ cm^{-3}$. Using equation (2-34), equation (2-33) becomes

$$\left(\frac{d_o^2}{e^{V_s} - V_s - 1}\right) = \left(\frac{2\kappa\varepsilon_o}{q^2}\right)\frac{(kT)^{-1/2}}{N_c'}\left\{\frac{\frac{1}{4}\left[\int_o^{V_s}\frac{(1 - e^V)\,dv}{F(v,o)}\right]^2}{e^{V_s} - V_s - 1}\right\}\exp\left[\frac{(E_c - E_F)b}{kT}\right]$$

(2-35)

This equation is quite useful in the analysis of experimental data . Assuming some particular energy-band structure, $\left(\frac{d_o^2}{e^{V_s} - V_s - 1}\right)$ may be calculated theoretically; this term, as a function of temperature, may be compared directly with experiment. The reason for the particular form of equation (2-35) becomes apparent when the limit of complete ionization is considered: in this case, the term $\frac{\frac{1}{4}\left[\int_o^{V_s}\frac{(1 - e^V)\,dv}{F(v,o)}\right]^2}{e^{V_s} - V_s - 1}$ approaches a value of 1; as well, for a one donor system $n_b \approx N_D$. Under these conditions, as will be shown in section

2.8, $\left(\frac{d_o^2}{e^{v_s} - v_s - 1}\right)$ is linear with temperature; any deviations from linearity can be ascribed to the effects of the donor levels.

The theory being presented here does not attempt to obtain the form of $v_s(T)$. Rather, the experimentally-determined values will be used in equation (2-35) to form theoretical curves. This gap between theory and experiment cannot be avoided unless the nature of the surface states is well known.

In Fig. 2-4 is seen the effect of partially ionized donor levels. For this plot of $\left(\frac{d_o^2}{e^{v_s} - v_s - 1}\right)$ versus KT a bandgap of $E_c - E_v = 2.42$ eV was assumed, with single donor and acceptor levels located at $E_c - E_D = 0.03$ eV and $E_A - E_v = 0.01$ eV, respectively; values of $g_D = 2$, $g_A = 2$ and $u_b = \infty$ were also used. The values of $v_s(T)$ used were given by $v_s = 0.66 - \frac{0.05\ eV}{kT}$; the exact position of E_F was determined numerically using equation (2-10). This plot is relatively insensitive to the values selected for g_A and N_A.

A comparison of these results with experiment appears in Chapter 4.

2.7 Van der Pauw Method of Conductivity Measurement

The measurement procedure thus far has been a two-probe technique; experimentally there is the possibility of contact

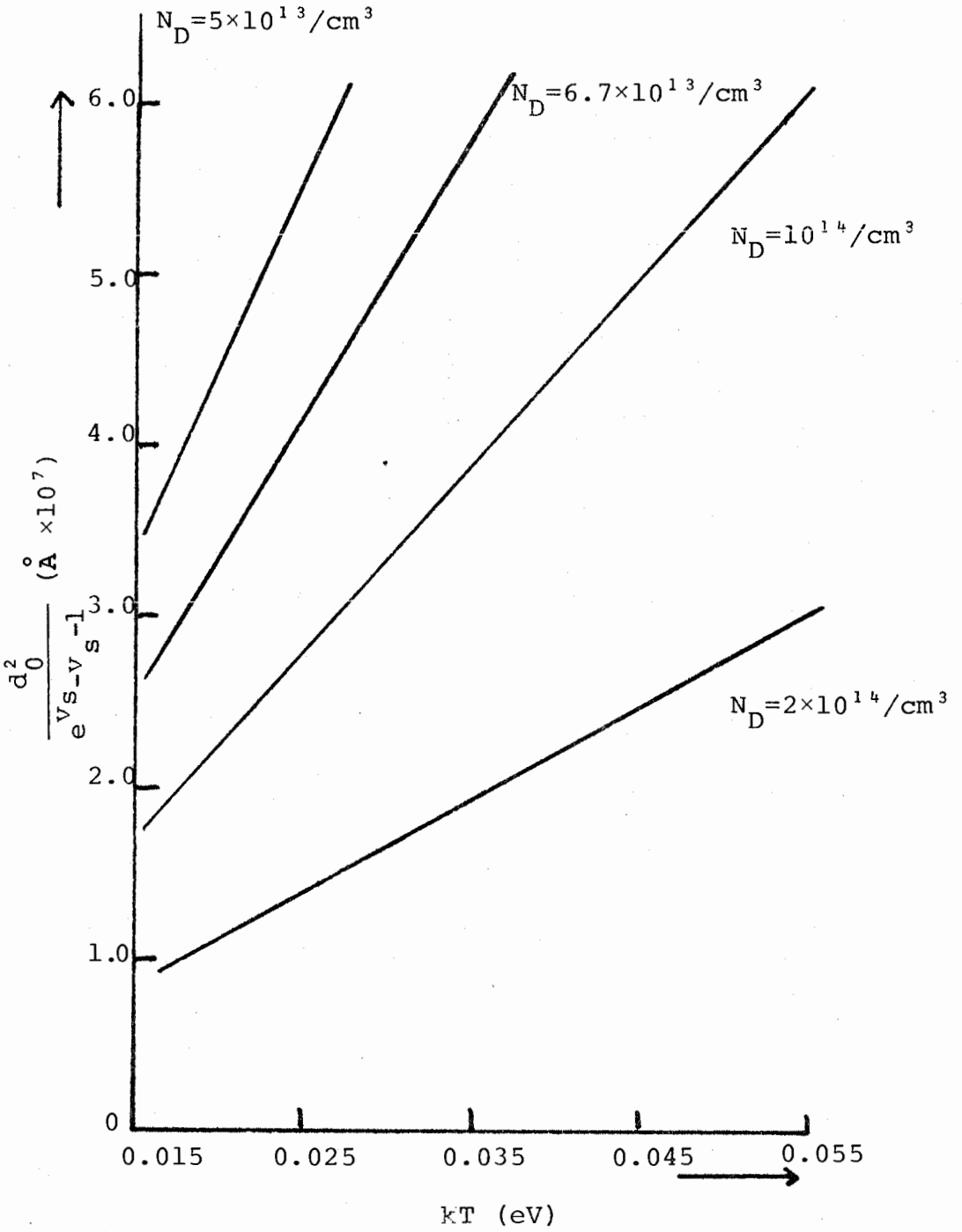

Figure 2-4. Theoretical variation of $\frac{d_0^2}{e^{v_s}-v_s-1}$ with temperature.

resistances developing between the sample itself and the attached contacts. A different set-up--a four-probe technique--can be used which eliminates this problem: this is the so-called Van der Pauw technique[18]. Other four-probe methods are described in the paper by Kataev, et al.[19]

The basis for this method is the following theorem. Consider a thin (two-dimensional), homogeneous, and simply connected sample of arbitrary shape, as shown in Fig. 2-5a; it is allowed to have an arbitrary small thickness d, and a constant conductivity σ. A, B, C and D are point contacts on the circumference of the sample. A resistance $R_{AB,CD}$ is defined as the ratio of the voltage drop $V_D - V_C$ between contacts D and C, to the current I_{AB} flowing from A to B; a resistance $R_{BC,DA}$ is similarly defined. Van der Pauw shows that

$$\frac{1}{\sigma} = \frac{\pi d}{\ell n 2} \frac{(R_{AB,CD} + R_{BC,DA})}{2} f\left[\frac{R_{AB,CD}}{R_{BC,DA}}\right] , \qquad (2\text{-}36)$$

where the function f depends only on the ratio of $R_{AB,CD}$ to $R_{BC,DA}$, and is a solution of

$$\frac{R_{AB,CD} - R_{BC,DA}}{R_{AB,CD} + R_{BC,DA}} = \frac{f}{\ell n 2} \operatorname{arc\,cosh}\left[\frac{\exp\left(\frac{\ell n 2}{f}\right)}{2}\right]. \qquad (2\text{-}37)$$

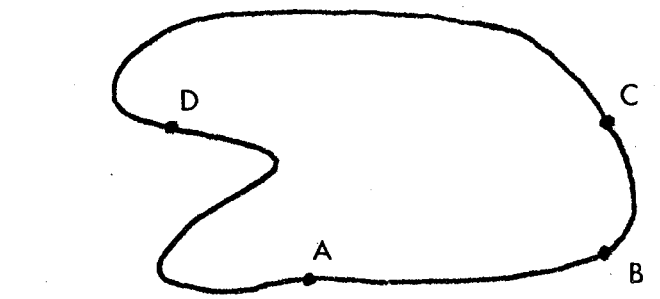

(a)

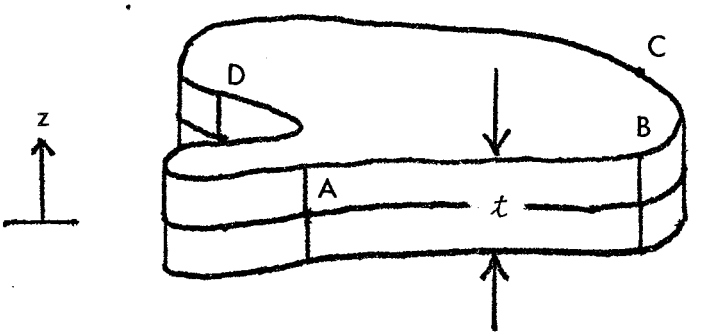

(b)

Figure 2-5. The geometries used for Van der Pauw's theorem for (a) the two-dimensional case, and (b) the extension to three dimensions.

The function f equals one when $R_{AB,CD} = R_{BC,DA}$, and otherwise is less than one; it is essentially a geometric factor.

Thus far, only a two-dimensional analysis has been given. This will now be extended to the three-dimensional sample sketched in Figure 2-5b; to allow for space-charge conditions the conductivity is a function of position, $\sigma(z)$, and the sample is considered to be a pile of infinitessimally thin layers, of thickness dz. The current flow (except for a negligible edge effect within a distance L of the circumference) will be parallel to these planes: equations (2-36) and (2-37) will hold for each of the planes, with d replaced by dz, σ replaced by $\sigma(z)$, and $\frac{1}{R_{HI,JK}}$ replaced by the infinitessimal $d\left(\frac{1}{R_{HI,JK}}\right)$.

The function f, being geometric in nature, will be the same for each layer; likewise, the ratio of $d\left(\frac{1}{R_{AB,CD}}\right)$ to $d\left(\frac{1}{R_{BC,DA}}\right)$ is the same in each layer. It follows then that

$$\int_{-t/2}^{+t/2} \sigma(z)dz = \frac{\ell n\ 2}{\pi} \left(\frac{2}{R_{AB,CD} + R_{BC,DA}}\right) \frac{1}{f\left(\frac{R_{AB,CD}}{R_{BC,DA}}\right)}, \qquad (2\text{-}38)$$

where $R_{AB,CD}$ and $R_{BC,DA}$ are now the total measured 'resistances' of the sample. An alternate treatment of this problem may be found in the paper by Pavlov[20].

If the function $y_1(t)$ is introduced through

$$y_1(t) \equiv \left(\frac{2}{R_{AB,CD} + R_{BC,DA}}\right) \frac{1}{f\left(\frac{R_{AB,CD}}{R_{BC,DA}}\right)}, \qquad (2\text{-}39)$$

then equation (2-38) becomes

$$\frac{\ell n\ 2}{\pi}\ y_1(t) = \int_{-t/2}^{t/2} \sigma(z)\,dz \qquad (2\text{-}40)$$

Referring to equation (2-19), it is seen that the term $\frac{\ell n\ 2}{\pi}\ y_1(t)$ from a Van der Pauw measurement, is equivalent to $\frac{\ell}{\omega}\ G$ in the previous two-probe arrangement. Hence, if both types of measurements are performed on samples with the same composition and thickness, a comparison between the two may be made.

The analysis in the previous sections of theory applies equally well to both methods of conductivity measurement.

The Van der Pauw measurements have the advantage that measurements are not affected by contact resistances[18]. As well, such samples can be readily adapted to the study of the Hall effect in thin film semiconductors.

In the preceding discussion it was assumed that the four contacts were point-contacts. Realistically, the contacts must be of finite size. To reduce errors arising from this source the shape of the Van der Pauw units was chosen, experimentally, to resemble clover-leafs (see, for example, Fig. 3-4); the wedges removed from the originally circular shape will tend to make the contact region less important.

2.8 Approximate Solutions

2.8.1

Before considering some approximations of the previous equations it is convenient to collect the several assumptions already made in the theory, either implicitly or explicitly.

a.) Essential in the theoretical development are equations (2-5), (2-6) and (2-7), describing the statistics of semiconductors. It has been assumed that the Fermi level is sufficiently far removed from conduction and valence bands that the carriers may be represented by Boltzmann statistics; the case of degenerate free carrier distributions is analyzed and discussed by Seiwatz and Green[10].

b.) The region between the space-charge region and the surface proper, where the surface charge excess accumulates, is assumed to contribute little to conduction. Since most of the surface charge is effectively immobile, trapped in surface states, and since the surface layer is only Angstroms thick, this assumption seems appropriate. The surface potential, V_s, is the potential at the boundary between the surface and space-charge layers.

c.) The bulk energy-band structure, except for the location of E_F, is taken to be temperature independent, although allowance for variations could be made.

Other less fundamental assumptions include:

d.) The sample (see Fig. 1-1) is symmetric about z = 0.

e.) The mobility, μ, is assumed constant throughout the sample. This is discussed in section 2.4, and in other references such as Schrieffer[11], and Greene, Frankl and Zemel[21].

f.) The semiconductor described was n-type, only electrons contributing to conduction. This disallows values of the potential, v, too strongly negative since an inversion layer would result wherein hole conduction becomes dominant.

g.) A somewhat arbitrary division of donor levels into ionized and unionized classes was made. It is always possible to consider all donor levels as unionized, and hence increase accuracy.

h.) The surface potential, V_s, was assumed to be independent of sample thickness.

2.8.2

In strongly n-type semiconductors like CdS at room temperatures, where $kT \approx \frac{1}{40}$ eV and $(E_F - E_i)_b \approx 1.0$ eV, the bulk potential u_b is effectively infinite. More specifically, when $u_b + v \gtrsim 3$ in n-type semiconductors, equation (2-18)

reduces to

$$F^2(v,v_o)\Big|_{u_b=\infty} = \left\{ e^v - e^{v_o} - (v-v_o) - \sum_i \left[\frac{N_{Di}}{n_b} \frac{(v-v_o)}{1+\frac{1}{g_{Di}} e^{x_i}} - \frac{N_{Di}}{n_b} \ln\left(\frac{e^v+\frac{1}{g_{Di}} e^{x_i}}{e^{v_o}+\frac{1}{g_{Di}} e^{x_i}} \right) \right] \right\}, \quad u_b+v \gtrsim 3; \quad (2\text{-}41)$$

and equation (2-31) reduces to

$$F^2(v,0)\Big|_{u_b=\infty} = \left\{ e^v - v - 1 - \sum_i \left[\frac{N_{Di}}{n_b} \frac{v}{1+\frac{1}{g_{Di}} e^{x_i}} - \frac{N_{Di}}{n_b} \ln\left(\frac{e^v+\frac{1}{g_{Di}} e^{x_i}}{1+\frac{1}{g_{Di}} e^{x_i}} \right) \right] \right\}, \quad u_b+v \gtrsim 3 \quad . \quad (2\text{-}42)$$

This approximation, although simplifying numerical calculations, does not yield an analytic expression for $2d_o$--a further assumption can do this.

2.8.3

If all the donors in the n-type semiconductor are completely ionized increased simplification of the previous formulae results. Under these conditions, the charge neutrality condition in the bulk (see equation 2-4) may be

written

$$n_b + \sum_j N_{Aj} = p_b + \sum_\ell N_{D\ell} \quad . \tag{2-43}$$

In CdS, however, with its large band-gap, the bulk hole density is negligible, so that

$$n_b \approx \sum_\ell N_{D\ell} - \sum_j N_{Aj} \quad . \tag{2-44}$$

The Fermi level is obtained from this using equation (2-5):

$$(E_c - E_F)_b \approx kT \ln \left[\frac{N_c}{\sum_\ell N_{D\ell} - \sum_j N_{Aj}} \right] \quad . \tag{2-45}$$

Equation (2-42) may now be simplified; each donor level is relatively near the conduction band, so if $N_c >> \left(\sum_\ell N_{D\ell} - \sum_j N_{Aj} \right)$ then e^{x_i} becomes large, and equation (2-42) becomes

$$F^2(v,0) \approx e^{v} - v - 1 \quad , \quad \text{for } N_c >> \left(\sum_\ell N_{D\ell} - \sum_j N_{Aj} \right). \tag{2-46}$$

Equation (2-30) is now easily integrated to give

$$d_{o/L} = \pm \sqrt{2}\,(e^{v_s} - v_s - 1)^{\frac{1}{2}} \quad , \tag{2-47}$$

and combining equations (2-47), (2-33) and (2-44), then

$$\frac{d_o^2}{e^{v_s} - v_s - 1} = \frac{2\kappa\varepsilon_o}{q^2 \left(\sum_\ell N_{D\ell} - \sum_j N_{Aj} \right)} \, (kT) \quad . \tag{2-48}$$

Thus, under the appropriate approximations, the term $\frac{d_o^2}{e^{v_s}-v_s-1}$ is proportional to the temperature; these conditions include nearly complete donor ionization, large u_b, and an effective density of conduction states N_c much greater than $(\sum_{\ell} N_{D\ell} - \sum_{j} N_{Aj})$. It is noted that complete donor ionization is not sufficient to give equation (2-48).

These approximations substantiate the claims made in section 2.6, and in particular, the use of the term $\frac{d_o^2}{e^{v_s}-v_s-1}$ to evaluate experimental data.

3. Experimental Technique

3.1 Introduction

To observe the conductance versus thickness curves described in the theory it is necessary to have several semiconducting films of the same composition but with varying thicknesses. This was achieved by evaporating, in vacuum, cadmium sulphide onto a prepared glass slide: suitable masks allowed several samples to form on the same slide, while a moving shutter enabled the thicknesses to be varied in a uniform manner. Both two-probe units, as in Fig. 1-1 (henceforth termed 'conductance units'), and Van der Pauw units were produced on the same slide. Suitable surrounding layers of insulators, and the necessary electrical contacts, were also vacuum evaporated onto the slide.

Measurements of the various resistances were then made in a prepared measurement chamber, under a rough vacuum.

The experiment may be broken into three stages. The first is the preparation of the glass slides; this is followed by the vacuum deposition of CdS and other materials onto the slides; this is followed by the various measurements on the completed device in the measurement chamber. Further discussion of each of these steps follows.

3.2 Preparation of Substrates

Type 7059 Corning glass slides were used for the substrates; these are two inches square and 1/32" thick. This glass is an alumino-borosilicate, being virtually sodium free--its resistivity is greater than 10^{12} Ωcm at 300°C.

The glass slides were ultrasonically cleaned in a detergent solution (usually Sparkleen) for five minutes, then rinsed in hot running water for 15 minutes. Four more ultrasonic washes, each for five minutes, followed, the first two in acetone, the last in ethanol. After drying in running nitrogen gas the slides were clamped together in pairs (using small metal clips) and stored in a dessicator.

To allow the substrate temperature to be controlled during the CdS evaporation a nichrome film, approximately 800 Å thick, was first evaporated onto the back face of the glass slide (the good side of the glass slide still being protected by the other slide clamped to it); current passing through this resistance film would heat the substrate quite uniformly (variations within a spread of 5°C are estimated). The nichrome evaporation was done with a pressure of 10^{-5} torr, a boule formed from nichrome wire being heated to evaporation temperature with an electron beam gun (powered by a Sloan six/ten electron beam power supply). Electrical contacts were made to the nichrome film by evaporating onto two opposing edges

an 80 Å layer of chromium, followed by a 1000 Å protective covering of gold. Fig. 3-1 shows the back face of such a prepared slide.

A chromel-alumel thermocouple (made from #50 wires spot-welded together at their ends) was attached with torr-seal epoxy onto the nichrome film; the amount of epoxy used was minimal so thermal contact with the substrate was as good as possible, and so that temperature gradients in the nichrome film were minimized.

The voltage output of the thermocouple was used in a feedback circuit to drive the nichrome current source. In this study, substrate temperatures of 70°C up to 170°C were used.

3.3 The Vacuum Deposition of Thin Films

3.3.1 The Vacuum System

Fig. 3-2 shows the arrangement of the essential device within the evaporator/vacuum system. The type 3176 NRC vacuum system and evaporator was capable of achieving 10^{-7} torr.

The substrate is mounted in place at the top of the assembly, being held by four plastic screws; the gold strips on the nichrome film make contact with two spring-loaded mounts. The thermocouple leads are spot-welded onto larger, permanent connectors within the assembly. All sets of electrical leads leave the assembly through hermetic seals within the vacuum collar.

Figure 3-1. Reverse face of substrate after nichrome evaporation.

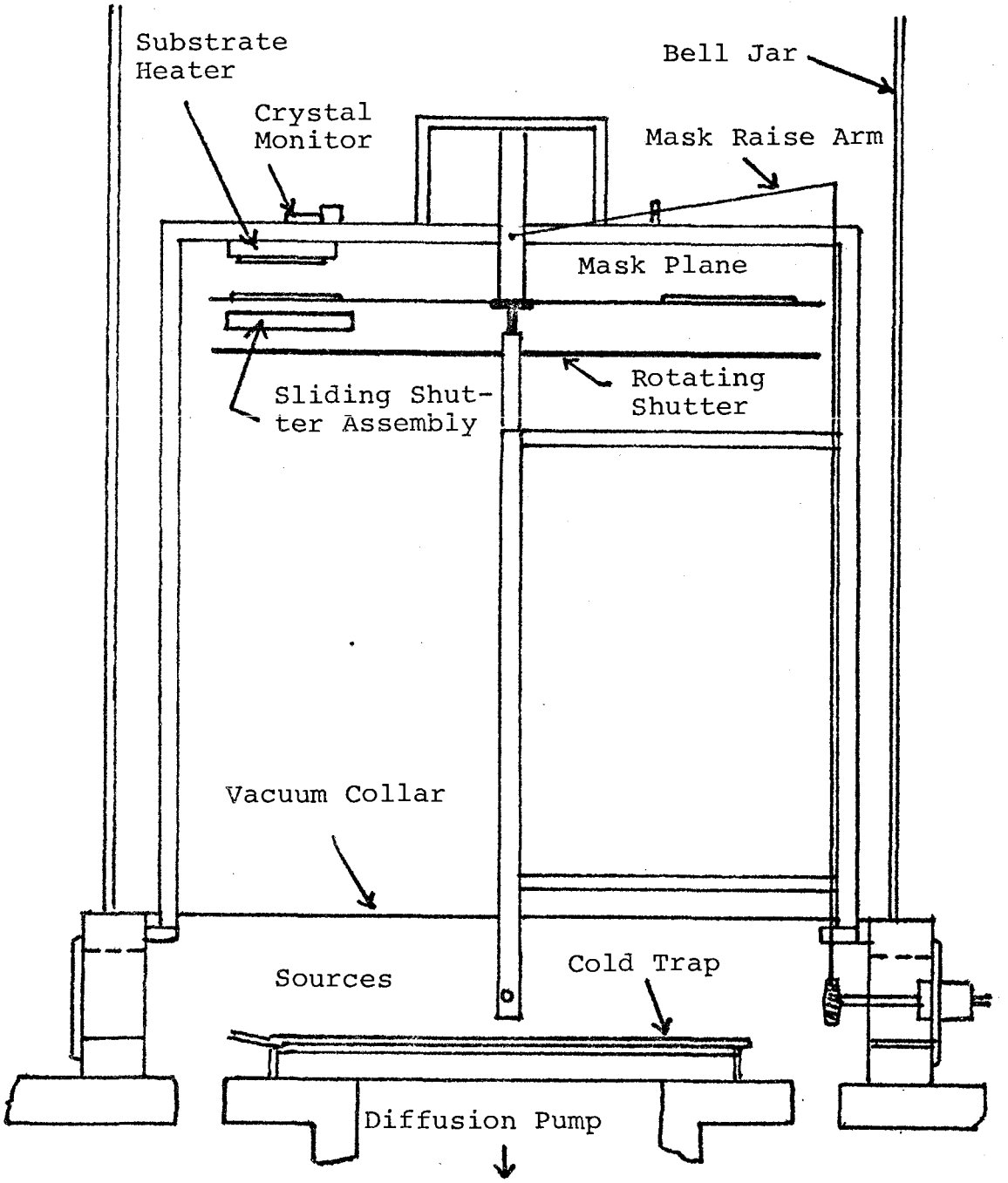

Figure 3-2. Details of the evaporator assembly.

Mounted just beside the substrate is a quartz crystal used to monitor the aggregate thickness of the films being evaporated. The resonant frequency of the crystal decreases approximately linearly with the added mass of the upward-streaming evaporant[22]. Knowing the calibration factors--a partial list of which appears in O'Hanlon's thesis[22]--between change in resonant frequency and thickness of film deposited, the thickness evaporated can be controlled.

Each of six different masks can be swivelled into position directly beneath the substrate; they are mounted on a plate which is rotated using controls outside the system. The masks themselves were made from 0.005" beryllium-copper foil by an etching technique described elsewhere[22]. The mask plate itself could be dropped $\frac{1}{2}$" to allow easy swivelling, or raised to within 1 mm of the substrate; guidepins ensured reproducible aligning of the substrate to within 0.001".

Below this is a movable shutter which can be pulled slowly across the face of the substrate--this is used to vary the thicknesses of the different samples. It is operated by a six revolutions/hour synchronous motor situated outside the vacuum assembly. A second shutter set so as to rotate about the vertical axis, could be swung between the substrate and evaporator sources whenever called for.

3.3.2 The Evaporator Sources and Materials

The various crucibles, holding the materials to be evaporated, are located at the bottom of the bell jar. They are heated either by the passage of current through a tantalum heater, or with an electron beam gun.

The principal material being investigated in this study was cadmium sulphide. High-purity Grade A crystals supplied by Eagle-Picher were ground up into chunks having dimensions less than 0.1 inches, and placed into a cylindrical boron nitride crucible; this, in turn, was set up in a tantalum heater. A sketch of this assembly is shown in Fig. 3-3. Shown also is the boron nitride cap and baffle used to prevent the ejection of solid CdS particles from the crucible; an alternative to this is to use a glass wool plug.

The actual form of the deposited CdS film is strongly dependent upon evaporation conditions. The CdS film may be deficient in sulphur due to the different coefficients of adhesion of sulphur and cadmium to the substrate[22]. As shown by Shalimova, et al.[23], both the hexagonal (wurtzite) and cubic crystal structures of CdS may appear with substrate temperatures less than 200°C; the orientation of the crystallites making up the film is also dependent upon substrate temperature, and vacuum pressure. Hence, the reproducibility of results between different prepared substrates may not be

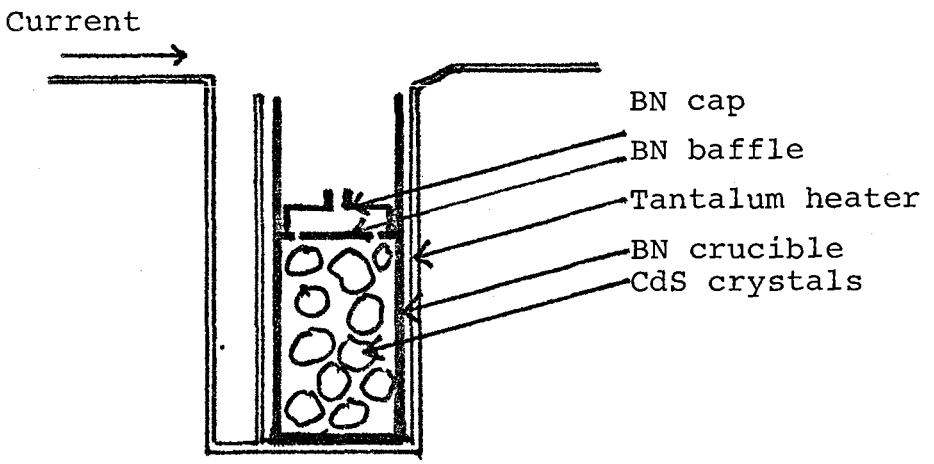

Figure 3-3. Details of the heater used for the evaporation of CdS.

good. However, the CdS films are being studied as a check on the theory, not to extract particular information about CdS. All that is required is that the various units evaporated onto a single substrate be uniform in composition and structure.

The different units of CdS film on a substrate typically varied from 1000 Å to 6000 Å in thickness.

On either side of the CdS film is evaporated a layer of insulator, usually about 3000 Å thick; an attempt is made to make these two layers as similar as possible, so that the surface potential V_s will be nearly the same on either side of the sample. Two different insulators were used, CaF_2 and SiO_x. CaF_2 is evaporated simply from an open boat of tantalum, and gives reliable films. The SiO_x films required a partial pressure of 10^{-4} torr of oxygen during the evaporation; they had a tendency to shatter if exposed to the atmosphere for more than a few weeks. SiO pellets are evaporated from a device similar in construction to that used for the CdS (although SiO is evaporated, the resultant film contains many species[22] such as SiO_2, Si, and Si_2O_3).

The electrical leads from the CdS units out to the edge of the substrate were 1000 Å of aluminum; a further 3000 Å of aluminum and 2000 Å of silver were added on the ends of these evaporated leads for strength--this is where external connections are to be made. The silver was

evaporated from an open tantalum boat, while the aluminum was evaporated from a large solid boule using an electron beam gun.

The substrate temperature was held at 170°C for the evaporation, except for the CdS film, for which the temperature was varied, values between 90°C and 170°C being used.

A completed substrate is shown in Fig. 3-4. The twenty darkish rectangles are the conductance samples, while the six clover-leaf patches are units for Van der Pauw measurements. The brighter lines leading out from these are the electrical contacts. There are forty external connections.

3.3.3 Associated Electrical System

The change in resonant frequency of the quartz monitor is measured with a frequency meter; an output from this is plotted on an X-Y recorder (Moseley 7001 AR Autograf) using a constant time sweep on the y-axis. The rate of evaporation can be controlled by observing the time rate change of frequency on this plot, or by using a Keithley electrometer connected through a differentiating circuit with the frequency meter output.

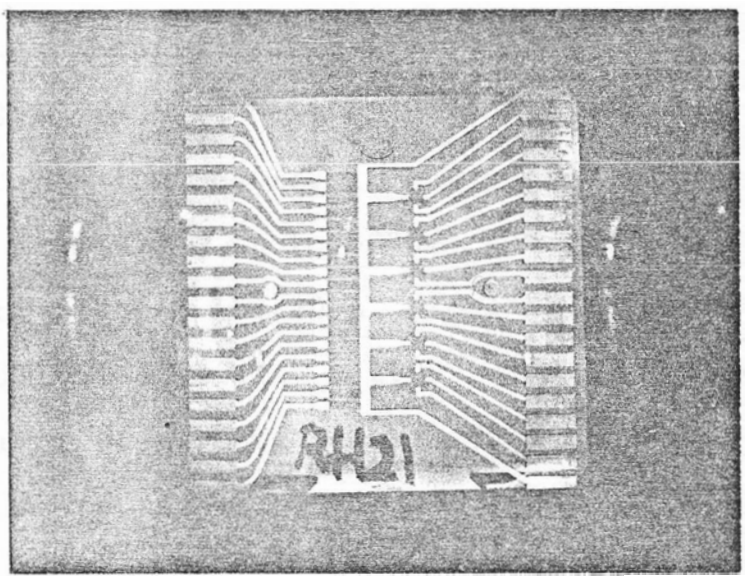

Figure 3-4. Front face of substrate after evaporation.

3.4 The Measurement Apparatus

A separate chamber is used for making resistance/conductance measurements on the prepared sample; it is pictured in Fig. 3-5. The temperature of the substrate is controlled with a thermo-electric module (Temptronix Model G9-65)--current applied to this Peltier-effect device causes a temperature drop across the module; it was possible to vary the sample temperature from -20°C up to 60°C. The thermo-electric module is powered by a Kepco 15v/20 a. bipolar operational power supply/amplifier, utilizing a 2000Ω thermistor imbedded in the copper plates between the module and the substrate.

Also in the copper plating is a copper-constantan thermocouple used to measure the sample temperature; it is connected externally to a Moseley 7100B strip chart recorder, so that the approach to thermal equilibrium can be observed.

The copper plates had been affixed to the thermo-electric module with a conducting epoxy, and the substrate mounted on the copper plating with thermal conducting grease. Two twenty-contact connectors clip onto either side of the substrate, matching the external contacts on the substrate; leads from these go to the measurement electronics. In Fig. 3-6 is shown the measurement chamber with a substrate mounted in position. When the cover plate is in place, the sample holder is virtually light-tight.

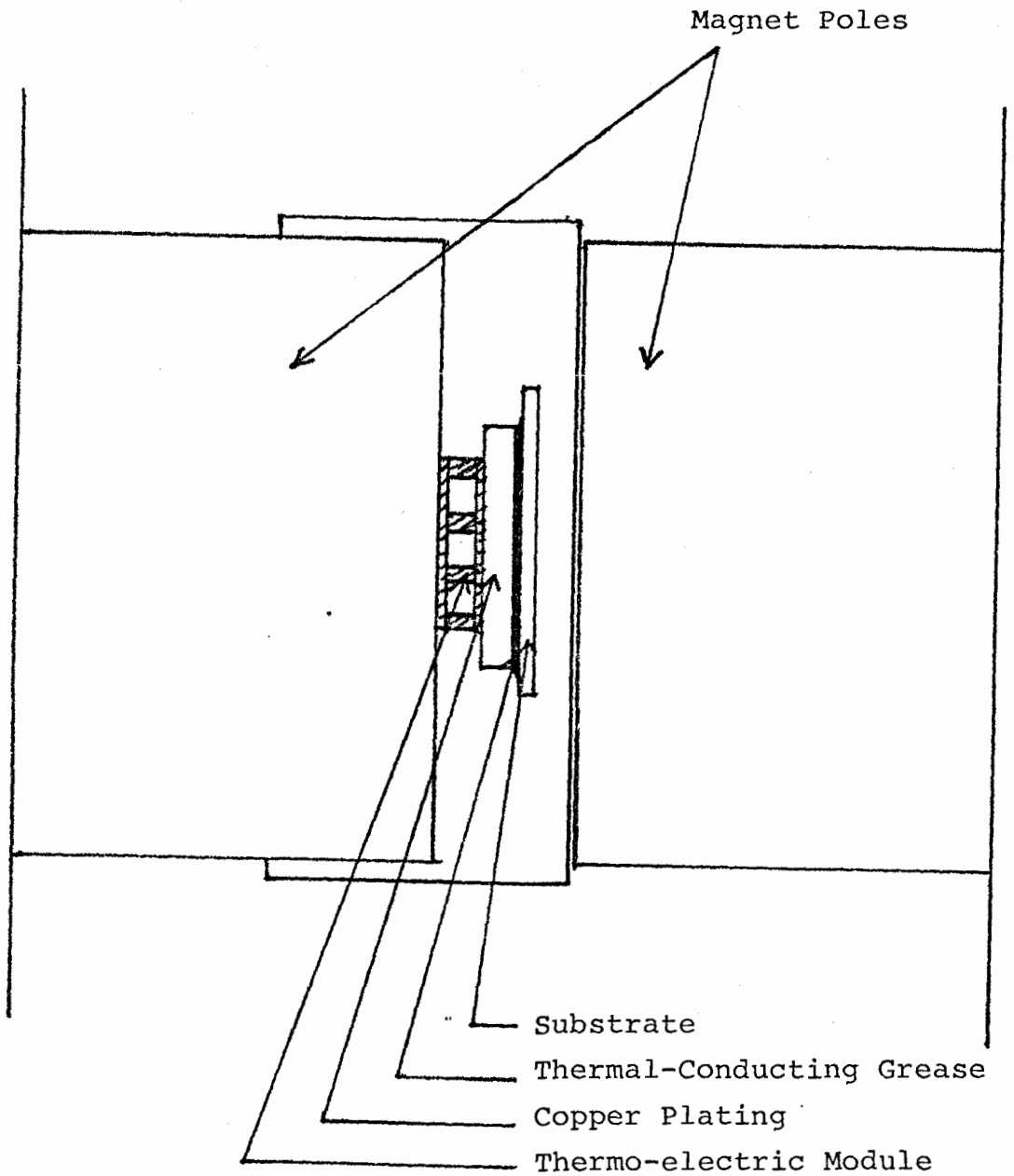

Figure 3-5. The measurement chamber.

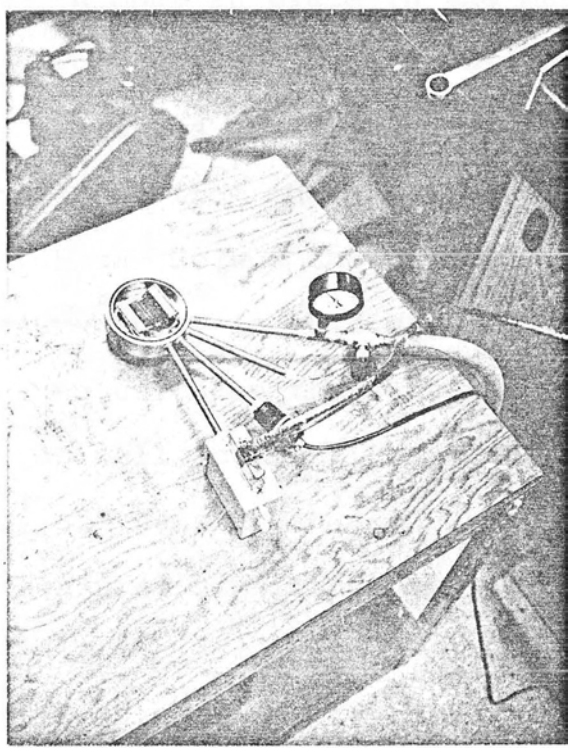

Figure 3-6. Measurement Chamber, showing positioning of the substrate.

The entire sample holder is mounted between the poles of a Cenco 4" electromagnet; Hall measurements on the Van der Pauw samples may be made when desired. Fig. 3-7 shows the measurement chamber in place in the magnet, and the associated electronics. The system is evacuated by a small roughing pump, pressures of about one torr being reached.

The forty leads from the substrate contacts enter a switchboard which can select the necessary leads for a particular measurement. In this way the resistances of the twenty conductance units on the substrate can be measured in succession; as well, current can be directed between two contacts of any of the six Van der Pauw units, with the voltage being measured simultaneously across the other two contacts.

The measurements of resistance, voltage and current are performed using type 602 and 610C Keithley electrometers; these devices are quite adequate for resistive measurements on samples having resistances up to $10^{10}\Omega$.

3.5 Experimental Procedures

As mentioned previously, the freshly cleaned glass slides are clipped face-to-face to avoid contamination; they remain like this during the nichrome evaporation, and while the thermocouple is being attached. They are separated only when the slide being used is placed in the

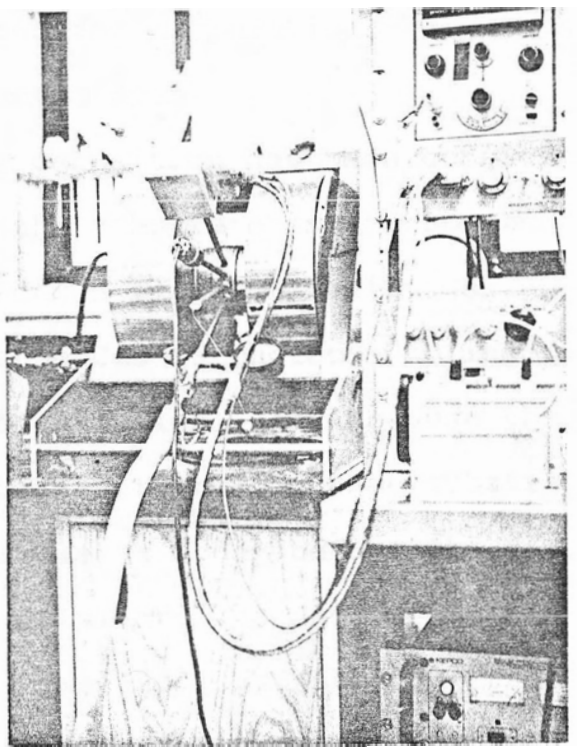

Figure 3-7. Measurement Chamber in place in the magnet.

vacuum system prior to the CdS evaporation.

Before evaporation, the substrate is baked at 200°C and 10^{-6} torr for an hour, to remove adsorbed gases. At the same time, the other crucibles are heated at temperatures just insufficient for evaporation--these bake-outs last for five or ten minutes each.

After the deposition has been completed and the substrate cooled, the substrate is transported to the measurement chamber under a flood of helium gas.

Because CdS is photoconducting (so time must be allowed for recombination), and because the measurement system is slow to stabilize thermally, the substrate is left undisturbed for at least a day before the resistance measurements are made; similarly, a wait of at least two hours is necessary each time the substrate temperature is altered.

Finally, when all electrical measurements are complete, the thickness of the CdS units on the substrate are determined using a Talysurf (Rank Organization) contacting-stylus, in which a diamond stylus is pulled across the units. Measurements are believed accurate to 300 Å.

4. Experimental Results

4.1 Introduction

In the course of this study, some twenty-one different substrates were prepared for measurement (labelled RH-3 up through RH-23). Some were made for comparison with the theory previously presented, while the others were used to explore the effects of varying certain evaporation parameters.

Two of the samples prepared for comparison with theory are discussed in sections 4.2 and 4.3, one of which shows an accumulation-type space-charge region, the other a depletion region. The ability of the theory to fit the experimental data is illustrated; the actual information concerning the CdS is incidental since the exact composition of the CdS film was not determined. Other samples, prepared for the same purpose, do not match with the theory--these will be discussed later in relation to the importance of various deposition conditions.

4.2 Films with Depletion Regions

In the prepared substrate, RH-13, an analysis of the conductance measurements showed a depletion layer to exist at the surface of the CdS films.

RH-13 was prepared by evaporating CdS onto the substrate at about 12 Å/second; the travelling shutter provided a gradient in thickness, the values ranging from 1000 Å to 6660 Å (an error of 300 Å, using the Talysurf contact-stylus, is estimated). The substrate temperature was 110°C during the CdS evaporation, and 170°C for the evaporation of the other materials.

On either side of the CdS film a layer of SiO_x approximately 3000 Å thick was evaporated; this deposition proceeded at 10 Å/second. Oxygen, with a partial pressure of 10^{-4} torr, was present during the evaporation of the SiO material.

Measurements of the conductance of he twenty rectangular units were made, and the values of $\frac{\ell}{\omega} G$ (see equation 2-22) calculated and plotted against the measured thicknesses. For this study, ℓ/ω was equal to 3.35. A few of the resultant conductance-thickness curves are shown in Fig. 4-1; one such curve is obtained for each of eleven different temperatures, ranging from -22.3°C to 61.0°C. Van der Pauw results were obtained only for a temperature of 16.8°C; these are included in Fig. 4-1, although a more thorough comparison of Van der Pauw and conductance techniques follows in section 4.6.

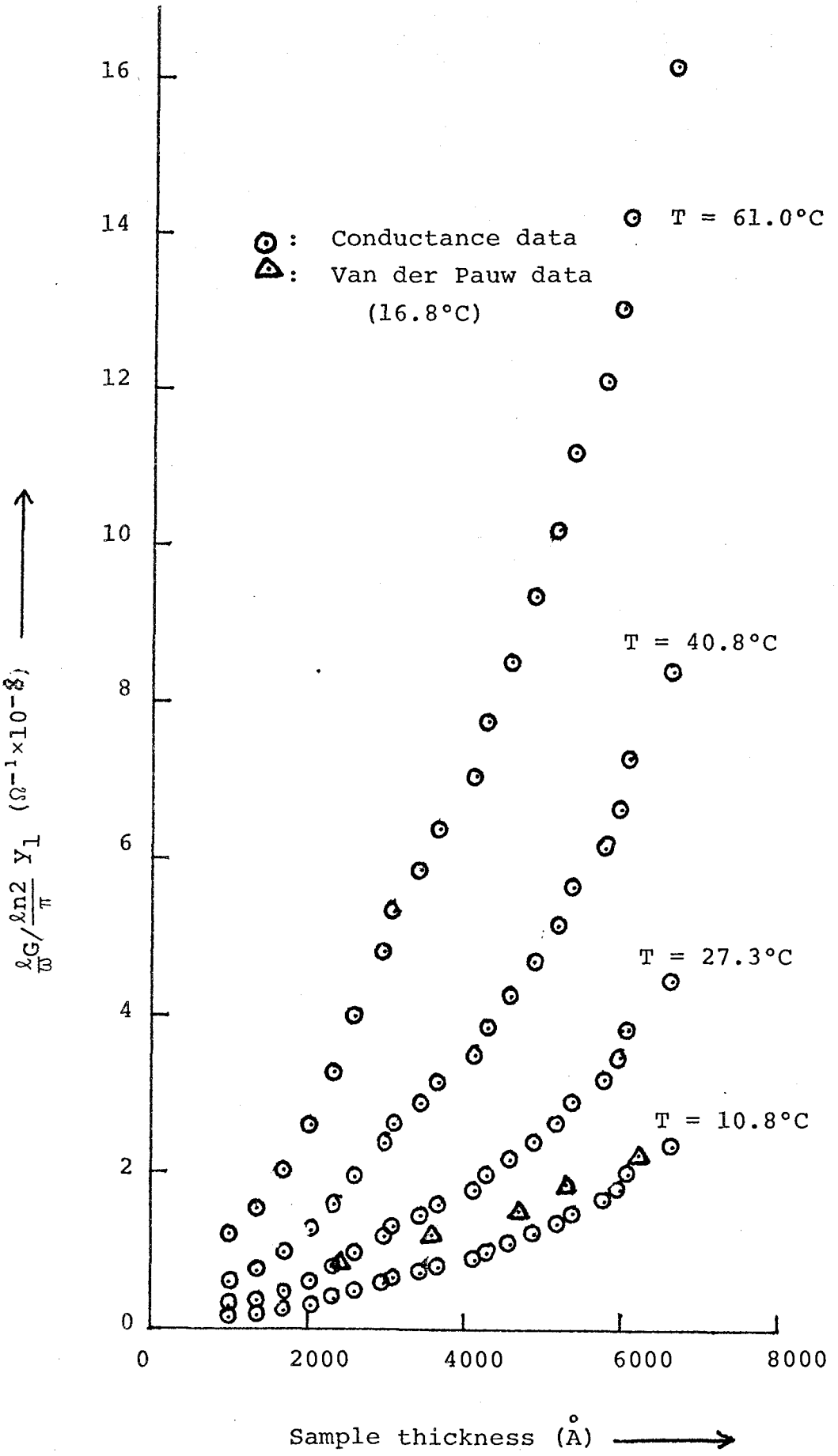

Figure 4-1. Conductance curves for RH-13, showing depletion

The conductance curves can be analyzed to obtain the parameters σ_b, v_s and $2d_o$. A least-squares fit was made, using the data points corresponding to thicknesses greater than 4600 Å; the values obtained for σ_b and $2d_o$ are tabulated in Table 4-1. Also listed are measured values of v_s: by equation (2-27) the conductance at small thicknesses is $\frac{\ell}{\omega} G = (\sigma_b e^{v_s}) t$; hence, using the first three data points of each curve, the initial slope $\sigma_b e^{v_s}$, and then v_s, can be determined.

For comparison, a similar analysis of the Van der Pauw curve gives $\sigma_b = (1.47 \pm 0.30) \times 10^{-3} \Omega^{-1} cm^{-1}$ and $2d_o = (2070 \pm 800)$ Å at 16.8°C.

As seen in the graph of $\ell n\, \sigma_b$ versus 1/kT, in Fig. 4-2, the bulk conductivity is described by $\sigma_b\ (T) \alpha \exp[-\frac{0.28eV}{kT}]$; a donor level at $E_c - E_D \geq 0.56eV$ could account for this relationship, but such a deep level is discounted. More likely the form of σ_b is dependent upon grain boundary effects[24], whereby a boundary between two crystallites of the film results in a potential barrier--this would cause an exponential dependence of the mobility with temperature.

Fig. 4-3 shows the temperature dependence of v_s. The best fit of the data is $v_s = (0.66 \pm 0.10) - \frac{(0.0500 \pm 0.004)eV}{kT}$;

Sample Temperature (°C)	σ_b ($\Omega^{-1}cm^{-1}\times10^{-3}$)	$2d_o$ (Å)	v_s
61.0	11.9	2250	-1.085
52.5	9.11	2340	-1.129
40.8	6.16	2410	-1.181
33.6	4.83	2480	-1.221
27.3	3.84	2540	-1.259
17.5	2.66	2660	-1.335
10.8	2.05	2700	-1.376
1.7	1.43	2790	-1.443
-7.0	1.00	2890	-1.522
-14.0	0.731	2940	-1.585
-22.3	0.516	3040	-1.670

TABLE 4-1. Bulk conductivity, $2d_o$, and the reduced surface potential of RH-13 units at various temperatures.

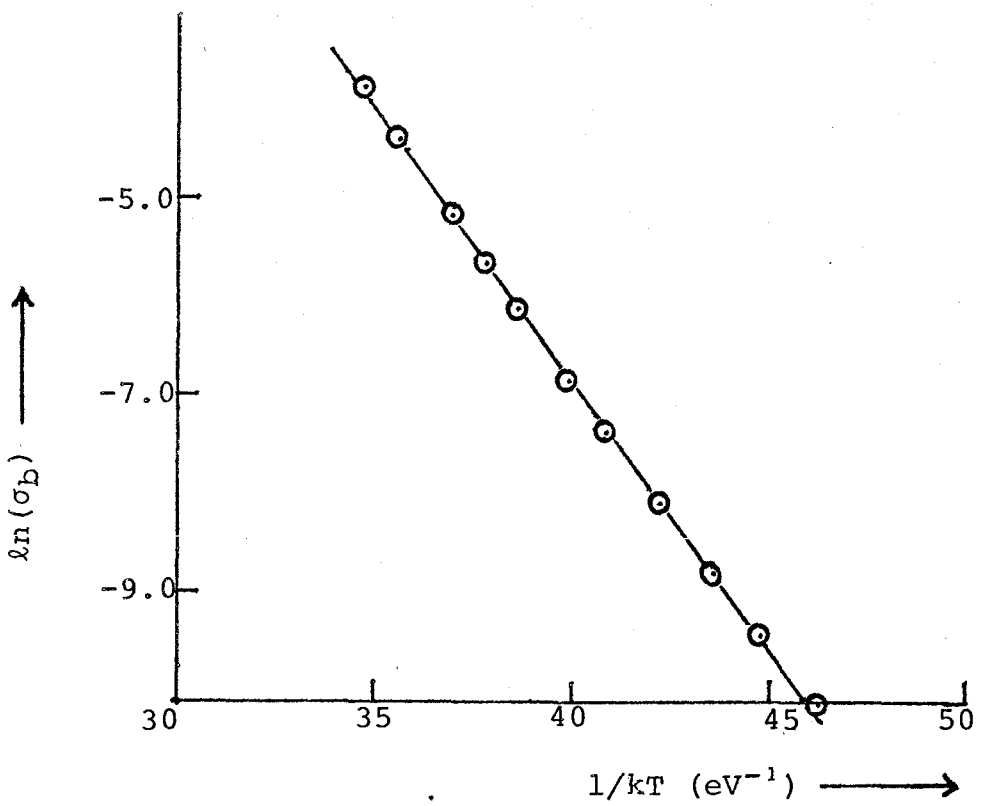

Figure 4-2. Bulk conductivity vs inverse temperature for RH-13.

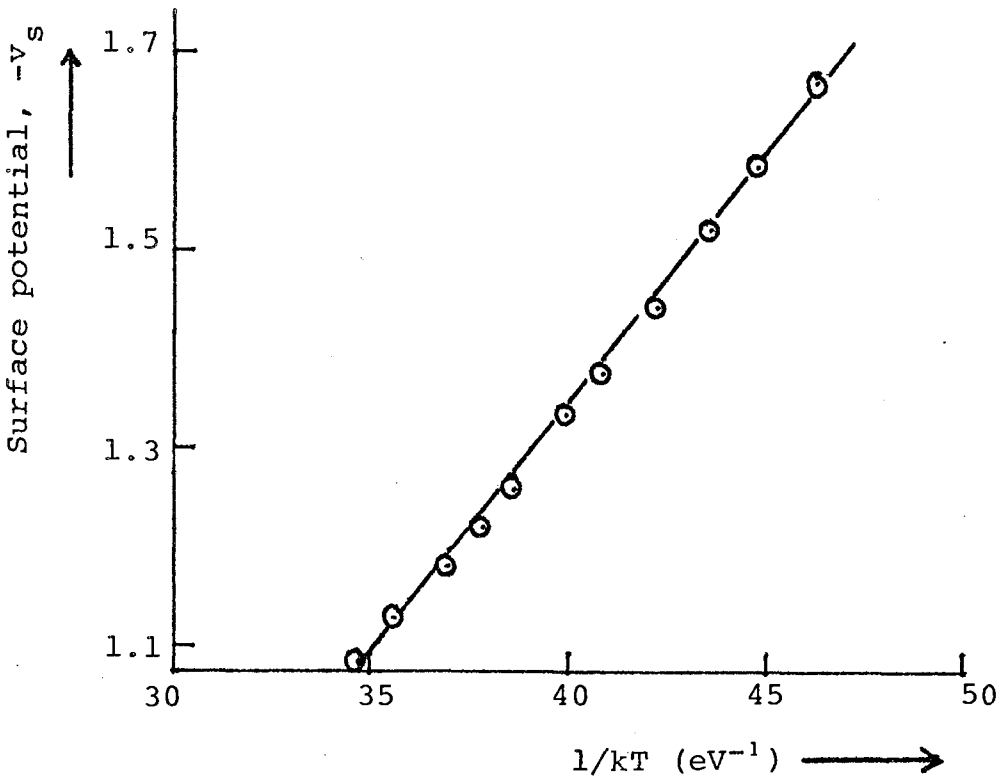

Figure 4-3. Reduced potential vs. inverse temperature for RH-13.

in the experiment, the errors due to conductance and temperature measurements are swamped by the $\pm$ 300 Å error in thickness measurements. It is found by error analysis that the uncertainties in thicknesses will affect only the intercept, and not the slope, of the v_s versus 1/kT graph; it is for this reason that error bars are not included for the ordinate.

The dependence of $\frac{d_o^2}{e^{v_s}-v_s-1}$ on temperature is shown in Fig. 4-4. As with the v_s data, the dominant source of error is the thickness measurements; however, since each data point of Fig. 4-4 (corresponding to the same set of conductance units, but at a different temperature) is affected by the errors in thickness in a related fashion, the use of error bars is ambiguous. That is, variations in the set of thickness measurements for the substrate samples may cause the curve of Fig. 4-4 to move by large amounts, but always so that the basic shape is relatively unchanged. The error bars used, then, show the estimated variation in each data point relative to the others; the subsidiary curves, labelled 1A and 1B, show the extremes in the behaviour of the entire curve as allowed by the errors in the thickness measurements.

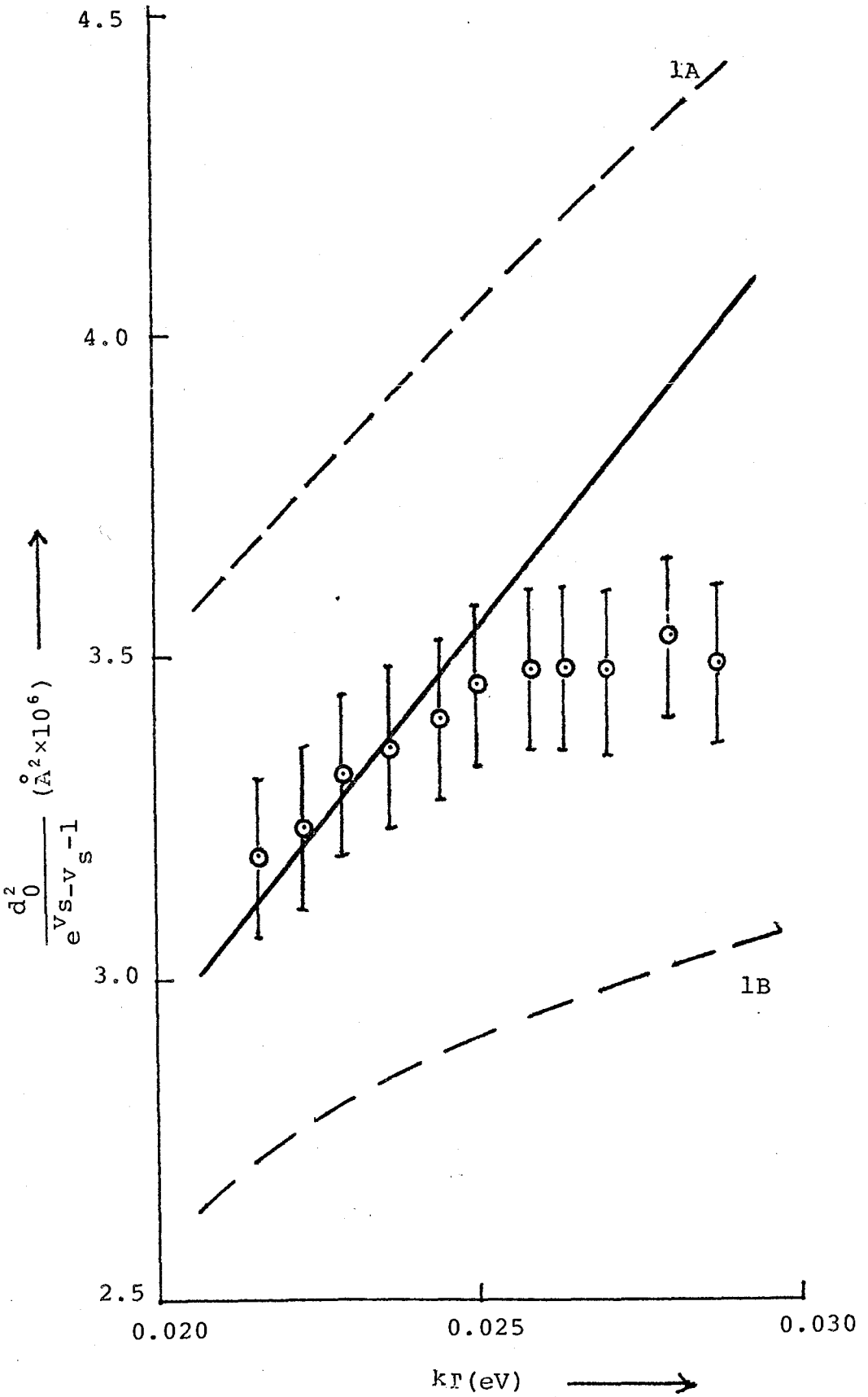

Figure 4-4. The term $\frac{d_0^2}{e^{v_s-v_s-1}}$ vs. k_T, for RH-13.

As seen in section 2.8.3, at sufficiently high temperatures (but not so high that the semiconductor becomes intrinsic) the term $\frac{d\delta^2}{e^{v_s}-v_s-1}$ is expected to become linear with temperature, with a slope $\frac{2\kappa\varepsilon_o}{[\Sigma_\ell N_{D\ell}-\Sigma_j N_{Aj}]q^2}$

From Fig. 4-4 then, it is found that the net donor concentration is given by $[\Sigma_\ell N_{D\ell} - \Sigma_j N_{Aj}] = (9 \pm 2) \times 10^{14}$ cm^{-3}. As well, the donor level cannot be situated too far from the conduction band, since effects due to incomplete ionization would become apparent; a comparison of theoretical curves (as in Fig. 2-4) with the experimental data suggests an upper bound of $E_C - E_D \lesssim 0.08$ eV.

The solid line on Fig. 4-4 is a theoretical curve using $N_D = 9 \times 10^{14}$ cm^{-3} (for a one donor model) and $E_C-E_D = 0.03$ eV. Other values used were $g_D = 2$, $u_b = \infty$, $\kappa = 10$ and $E_C-E_v = 2.42$ eV; the last two are values typical of CdS. The assumed form of the surface potential was the experimentally derived $v_s = 0.66 - \frac{0.05 \text{ eV}}{kT}$. The values of $E_A-E_v = 0.01$ eV and $g_A = 2$ used have a negligible effect on the theoretical curves.

4.3 Films with Accumulation Regions

The substrate RH-3 was prepared in much the same fashion as the previously-discussed RH-13, except that a substrate temperature of 170°C was used during the CdS evaporation.

Fig. 4-5 shows the variation of conductance with sample thickness. The form of these curves is indicative of an accumulation-type space-charge region, and hence, a downward bending of the energy bands at the surface (refer back to Fig. 1-2). An analysis of these curves, for the ten temperatures used, completes Table 4-2.

As with RH-13, the bulk conductivity depends exponentially on 1/kT, having the form $\sigma_b(T) \propto \exp\left[-\frac{0.26\ eV}{kT}\right]$; this activation energy is again attributed to grain boundaries.

The reduced surface potential, v_s, is shown in Fig. 4-6; the best linear fit is $v_s = (1.48 \pm 0.10) - \frac{(0.0204 \pm 0.0008 eV)}{kT}$.

Finally, Fig. 4-7 shows $\frac{d_o^2}{e^{V_s} - v_s - 1}$ plotted against temperature; an analysis similar to that made for RH-13 has been performed. Curves 2A and 2B show the approximate limits of the experimental curve, as determined by the error in the thicknesses; the error bars show the estimated error of one data point relative to the curve.

Analysis of the data on Fig. 4-7 gives estimates of $N_D = (8 \pm 2) \times 10^{14}\ cm^{-3}$ and $E_c - E_D \lesssim 0.05$ eV, for an assumed one donor model.

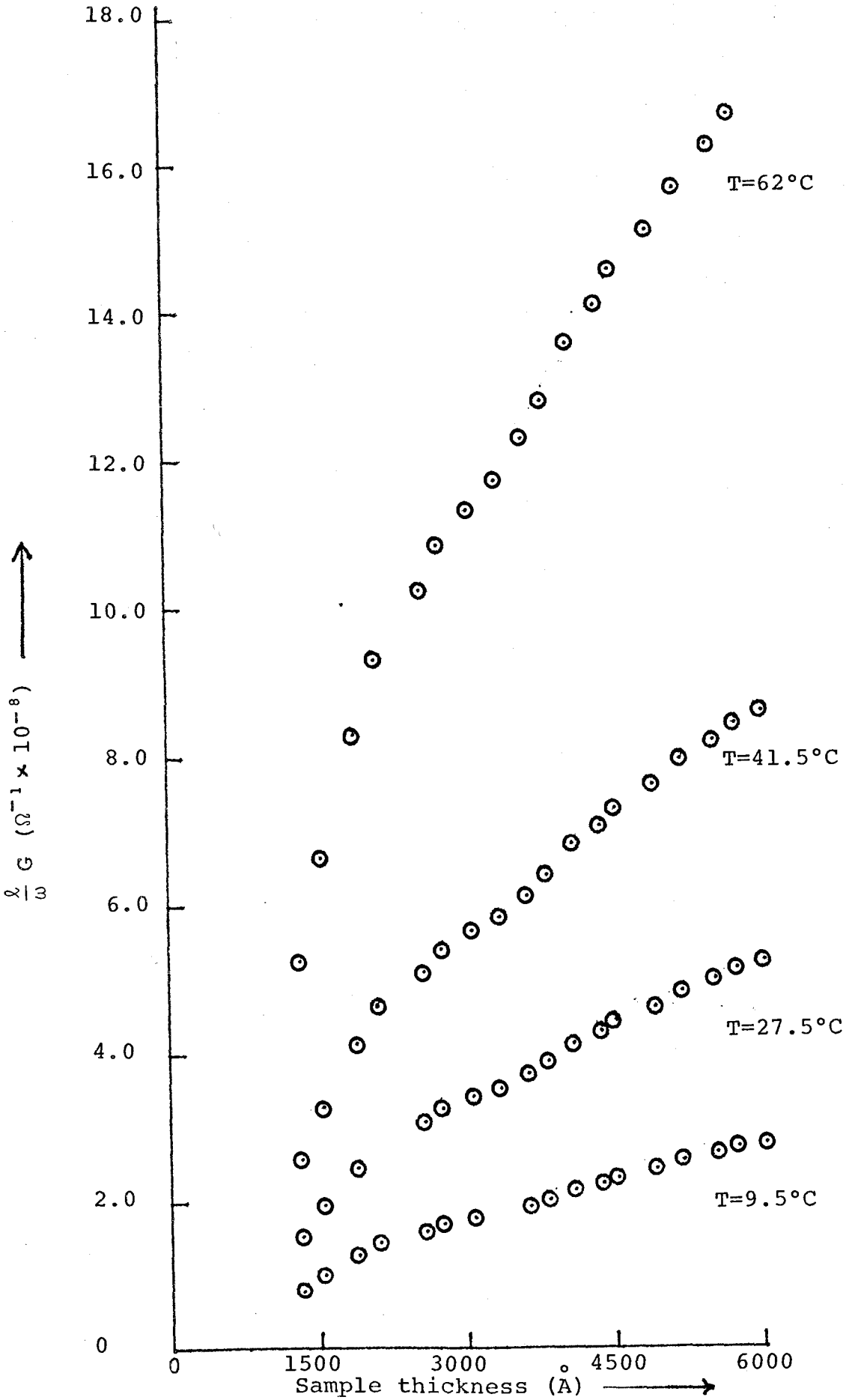

Figure 4-5. Conductance curves for RH-3, showing accumulation.

Sample Temperature (°C)	σ_b (Ω^{-1} cm^{-1} × 10^{-3})	$2d_o$ (Å)	v_s
62.0	2.05	2450	0.765
53.0	1.55	2360	0.742
41.5	1.06	2240	0.723
33.5	0.801	2210	0.718
27.5	0.653	2130	0.691
16.5	0.456	2000	0.665
9.5	0.362	1810	0.626
-0.5	0.249	1800	0.619
-8.5	0.177	1690	0.584
-16.0	0.133	1510	0.550

TABLE 4-2. Bulk conductivity, $2d_o$, and the reduced surface potential of RH-3 units at various temperatures.

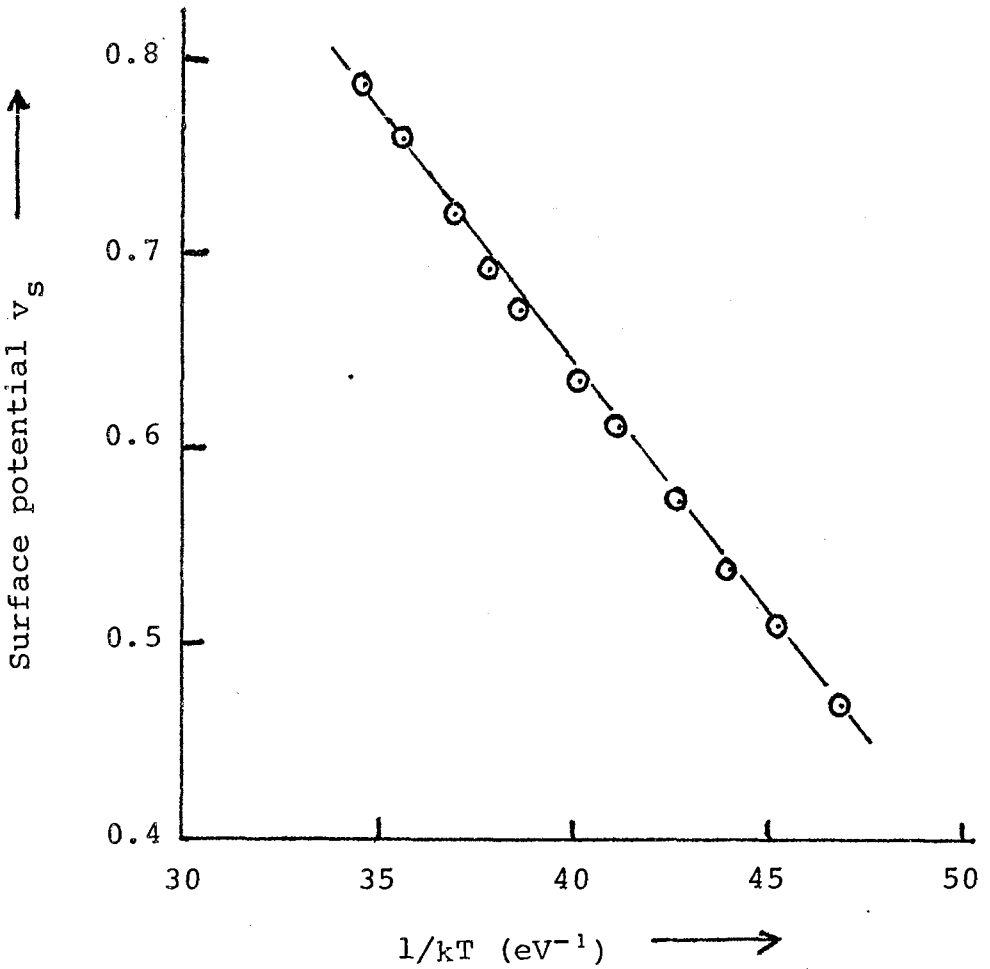

Figure 4-6. Reduced potential vs inverse temperature for RH-3.

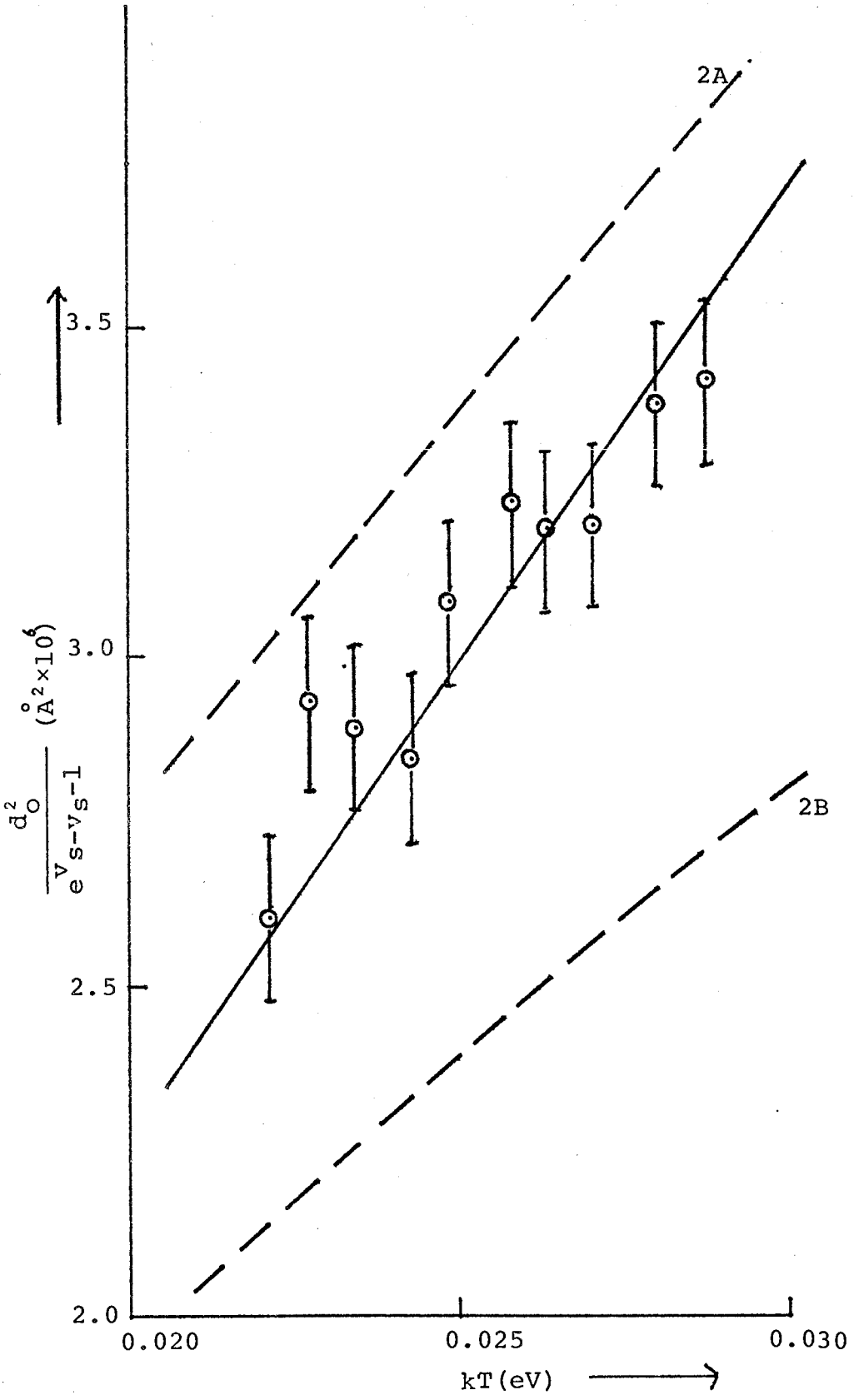

Figure 4-7. The term $\frac{d_o^2}{e^{v_s - v_s - 1}}$ vs. kT, for RH-3.

For a comparison with theory, Fig. 4-7 also includes a predicted curve (solid line) for which it was assumed that $N_D = 8 \times 10^{14}$ cm^{-3}, $E_c - E_D = 0.03$ eV, $g_D = 2$ and $u_b = \infty$; a dielectric constant of $\kappa = 10$ and bandgap of 2.42 eV were used. An assumed surface potential had the form $v_s = 1.48 - \frac{0.02 \text{ eV}}{kT}$.

4.4 Discussion of the Data

Figures 4-4 and 4-7 illustrate the capability of the derived theory to explain the experimental data; unfortunately, the large errors associated with the thickness measurements of thin films disallow a more precise comparison. As well, the material (CdS) and temperature range used tested only a small portion of the applicable theory. Using a combination of smaller band-gap material, lower temperatures and deeper-lying donor levels, future experiment may check the realm of incomplete donor level ionization.

A further experimental problem, discussed in section 4.5, is the variation in bulk conductivity over the units of the prepared substrate; this would also tend to increase errors for the parameters $2d_o$ and v_s.

The exponential variation of the bulk conductivity with $1/kT$, as demonstrated in Fig. 4-2, has been attributed to grain-boundary effects; the boundary between two crystallites

is the seat of a potential barrier, the energy bands shifting in a similar fashion as that for surface states. Each grain boundary will be surrounded on either side by an appropriate space-charge region. The size of crystallites in evaporated CdS films is strongly dependent upon evaporation conditions[25] and substrate treatment[26]; values of 2000 Å, could be expected. Since this is of the order of the extent of the space-charge region, L, the value of bulk conductivity measured cannot be expected to coincide with the single crystal value. Also, the actual conductivity will be a function of deposition conditions[27]; hence, the differing of σ_b, for RH-13 and RH-3, by a factor of five is easily accepted.

The form of the surface barrier, for both accumulation and depletion space-charge regions, was $v_s = |A| - |B|/kT$. This suggests that a semiconductor with a depletion layer may become an accumulation layer at sufficiently large temperatures (for example, an extrapolation of Fig. 4-3 suggests that RH-13 has an accumulation layer for $T \gtrsim 1000°K$); more likely, however, the linear form of v_s as a function of $1/kT$ is only approximate. More work experimentally and, especially, theoretically, must be performed before any conclusions may be drawn: throughout this thesis a consideration of the exact nature and behaviour of surface states has been omitted. Again, reference to Mark[8] or Heine[4] might be in order.

4.5 Variation in Bulk Conductivity across the Substrate

It has been presumed that the twenty conductance and six Van der Pauw units, deposited on a single substrate, have the same bulk conductivity. To check this, RH-18 was prepared in a fashion similar to that of RH-3 and RH-13, but without the use of the movable shutter: hence, all the units have the same thickness. The CdS, deposited at a substrate temperature of 150°C, was surrounded by 3000 Å layers of SiO_x.

Fig. 4-8 shows the resultant measured conductances for the various units. The conductance units are numbered 1 through 20, with the Van der Pauw units numbered 3, 6, 9, 12, 15, 18 (this designates their relative positions--see Fig. 3-4). For the conductance units the term $\frac{\ell}{w} G$ was plotted on the ordinate; for the Van der Pauw units, the equivalent (compare equation 2-1 and 2-40) term $\frac{\ln 2}{\pi} y_1$ was used; the unit number appears on the abscissa.

Although all samples are approximately the same thickness (5000 Å $\pm$ 6%), the conductivities may differ by as much as 50% across the substrate. Unless this variation can be accurately and consistently allowed for, the errors in the $\frac{d_o^2}{e^{v_s}-v_s-1}$: kT curves will be increased.

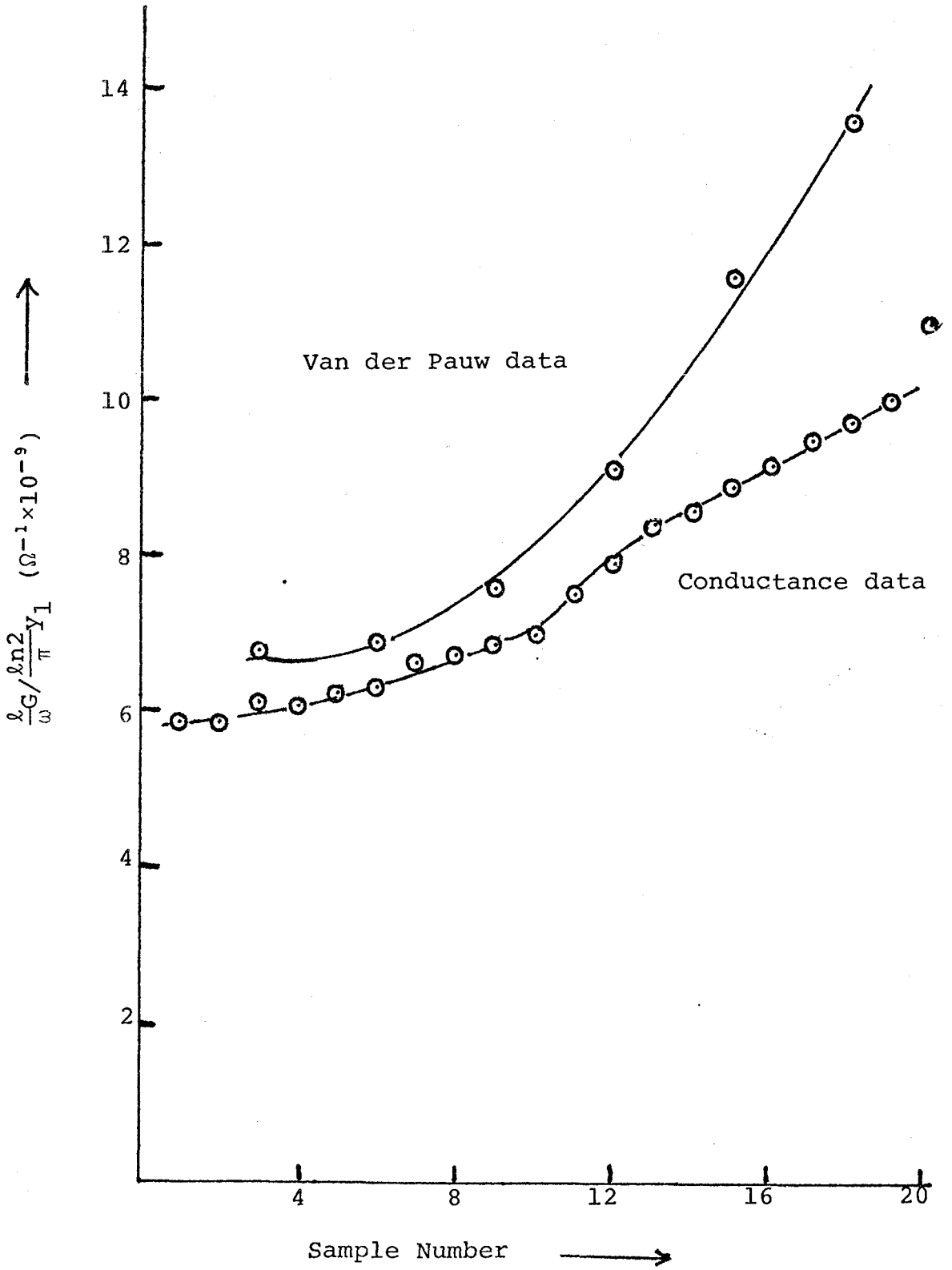

Figure 4-8. Variation in bulk conductivity over substrate

This local variation in conductivity can be explained by considering the manner in which CdS evaporates[22]:

$$CdS\ (solid) \rightarrow Cd\ (vapour) + \frac{1}{2} S_2 (vapour). \qquad (4\text{-}1)$$

The separate existence of both Cd and S_2 in the vapour stream and their differing coefficients of adhesion to the substrate allow for a non-stoichiometric formation of CdS. As well, varying degrees of reflection off the baffles (see Fig. 3-2) can account for the position-dependent stoichiometry (or bulk conductivity) evidenced in Fig. 4-8.

4.6 The Use of Four-Probe Conductivity Measurements

Two-probe conductivity measurements, discussed previously, are susceptible to errors due to contact resistances between the semiconductor film and the evaporated connections. This will tend to decrease the measured conductances, the effect being more dominant at the high conductance/large thickness portions of the G versus t curves.

The Van der Pauw technique, utilizing four probes, will eliminate this difficulty[18]. In the experiments the necessary size of the Van der Pauw units allowed only six such units to be constructed with each evaporation.

The experimental data of Fig. 4-8, presented previously, might suggest contact resistances developing in the two-probe units. However, the results of Fig. 4-9 show the opposite

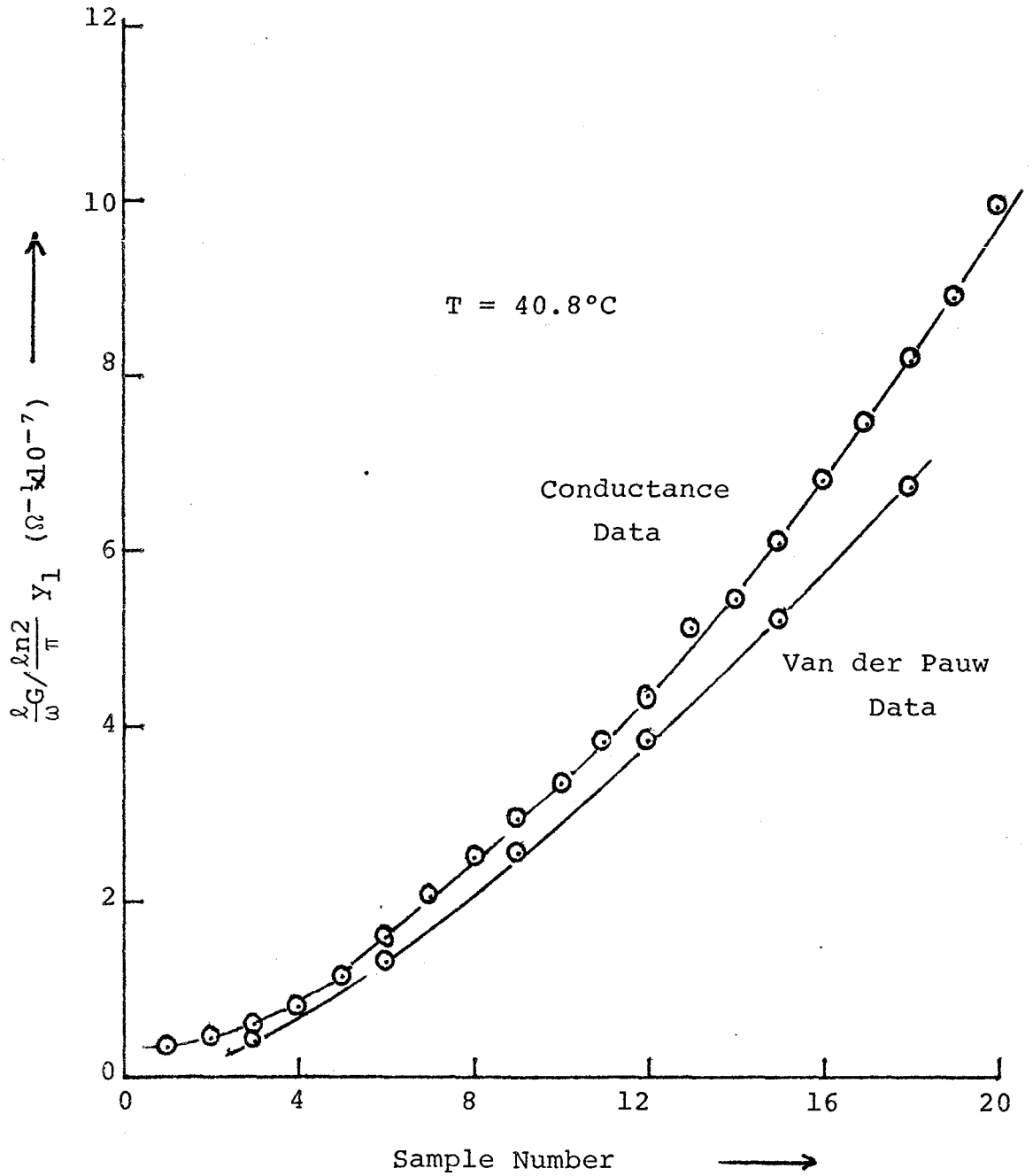

Figure 4-9. Comparison of Conductance and Van der Pauw measurements for RH-15.

effect--the Van der Pauw curves (plotting $\frac{\ln 2}{\pi} y_1$) are not above the conductance curves as would be expected. Fig. 4-9 is obtained from RH-15, prepared in the same fashion as RH-13 except for a substrate temperature of 90°C during the CdS deposition.

No conclusive evidence was found to suggest the formation of contact resistances in the two-probe conductance units. As well, the actual resistances being measured are relatively large--ranging from $10^7\Omega$ to $10^9\Omega$--so any contact resistances might be swamped. In this study, then, the observed difference between the two and four-probe measurements was assumed to be due to variations in bulk conductivity over the substrate.

In these experiments, more two-probe than four-probe units could be deposited on a single substrate; the determination of v_s, $2d_o$, and σ_b was then more accurate for the two-probe units.

5. Conclusion

In the theoretical portions of this study the effect of surface states on conduction in thin semiconducting films was described. The work of Kingston and Neustadter [9], Seiwatz and Green [10] and Mark [8] has been extended to include both the effect of incomplete donor level ionization, and the use of films of finite thickness (as opposed to the thick, or semi-infinite, models of most authors). The conductance of thin film slabs has been expressed theoretically as a function of film thickness, and a parameterization procedure introduced which allows an easy comparison with experimental data; the form of the theoretical relations also permits the determination of the degree of donor level ionization.

The experiments described in Chapter 4 could be interpreted quite well using the derived theory; the large errors associated with the measurement of film thickness, however, disallowed a more precise comparison. In future, related experiments, more simultaneous units must be constructed, or the thickness errors reduced; the use of optical interference techniques might be practical; another possible technique, still being developed for thickness measurements, is the use of a non-contacting field-emission

probe, as discussed by Young [28,29].

The precise nature of surface states was not considered; instead, their effects were characterized by a surface potential, V_s, the amount by which the energy bands are displaced, from their bulk locations, at the surface. The actual experimental determination of the surface states is a difficult problem at best [8].

Also arising out of the theory was a new method for measuring the surface potential, V_s, of thin film semiconductors. For this technique--described in Section 2.5--a number of conductance units, of varying thickness, are evaporated simultaneously on one substrate; the observed rate changes of conductance with thickness, for the limits of zero and infinite film thicknesses, can be used (via equation 2-27) to obtain $\frac{qV_s}{kT}$. This technique was found to be practical experimentally and, with refinements in the determination of film thickness, should prove useful in the future.

REFERENCES

1. J. Bardeen, Phys. Rev., 71, 717 (1947).

2. I. E. Tamm, Z. Phys., 76, 849 (1932); Phys. Z. Sowjet., 1, 733 (1932).

3. W. Shockley, Phys. Rev., 56, 317 (1939).

4. V. Heine, Phys. Rev., 138A, A1689 (1965).

5. J. Bardeen and S. R. Morrison, Physica, 20, 873 (1954).

6. H. Statz and G. A. DeMars, Phys. Rev., 111, 169 (1958).

7. A. Many, Y. Goldstein, and N. B. Grover, Semiconductor Surfaces, (North-Holland Publishing Company, Amsterdam, 1965).

8. P. Mark, Surface Sci., 25, 192 (1971).

9. R. H. Kingston and S. F. Neustadter, J. Appl. Phys., 26, 718 (1955).

10. R. Seiwatz and M. Green, J. Appl. Phys., 29, 1034 (1958).

11. J. R. Schrieffer, Phys. Rev., 97, 641 (1955).

12. S. G. Davison and J. D. Levine, "Surface States" in Solid State Physics, H. Ehrenreich, F. Seitz and D. Turnbull, Editors (Academic Press, 1970), Page 1.

13. See for example, C. Kittel, Introduction to Solid State Physics, 3rd Edition (Wiley and Sons, 1966), Ch. 9.

14. R. R. Haering and J. F. O'Hanlon, Proc. I.E.E.E., 55, 692 (1967).

15. J. Blakemore, Semiconductor Statistics, (Pergamon Press, 1962), Ch. 2.

16. S. M. Sze, Physics of Semiconductor Devices, (Wiley-Interscience, 1969), Page 34.

17. G. C. Dousmanis and R. C. Duncan, Jr., J. Appl. Phys. 29, 1627 (1958).

18. L. J. Van der Pauw, Phillips Res. Repts., 13, 1 (1958).

19. Yu. G. Kataev, L. G. Lavrent'eva, and I. P. Pogrebnyak, Sov. Phys. J., 12, 818 (1969).

20. N. I, Pavlov, Sov. Phys. - Semiconductors, 4, 1644 (1971).

21. R. F. Greene, D. R. Frankl, J. Zemel, Phys. Rev., 118, 967 (1960).

22. J. F. O'Hanlon, Ph.D. Thesis, Simon Fraser University (1967).

23. K. V. Shalimova, A. F. Andrushko, V. A. Dmitriev and L. P. Pavlov, Sov. Phys. - Cryst. 8, 618 (1964).

24. J. C. Anderson, Advances in Phys., 19, 311 (1970).

25. B. D. Galkin, N. V. Troitskaya, and R. D. Ivanov, Sov. Phys. - Cryst., 12, 766 (1968).

26. J. Dresner and F. V. Shallcross, J. Appl. Phys., 34, 2390 (1963).

27. R. S. Muller and B. G. Watkins, Proc. I.E.E.E., 52(I), 425 (1964).

28. R. D. Young, Rev. Sci. Instr., 37, 275 (1966).

29. R. D. Young, Physics Today, 42 (Nov. 1971).